# Spin state of two mononuclear iron(II) complexes of a tridentate bis(imino)pyridine N-donor ligand: Experimental and theoretical investigations

Yosef Bayeh, Patrik Osuský, Nathan J. Yutronkie, Róbert Gyepes, Assefa Sergawie, Peter Hrobárik, Rodolphe Clérac, Madhu Thomas

# Spin state of two mononuclear iron(II) complexes of a tridentate bis(imino) pyridine *N*-donor ligand: Experimental and theoretical investigations

Yosef Bayeh [a,b,c], Patrik Osuský [b], Nathan J. Yutronkie [d], Róbert Gyepes [e], Assefa Sergawie [a], Peter Hrobárik [b], Rodolphe Clérac [d], Madhu Thomas [a,c,*]

[a] *Department of Industrial Chemistry, College of Applied Sciences, Addis Ababa Science and Technology University, P.O. Box 16417, Addis Ababa, Ethiopia*
[b] *Department of Inorganic Chemistry, Faculty of Natural Sciences, Comenius University, Mlynská dolina CH-2, Ilkovičova 6, 84215 Bratislava, Slovakia*
[c] *Nanotechnology Centre of Excellence, Addis Ababa Science and Technology University, Addis Ababa P.O. Box 16417, Ethiopia*
[d] *Univ. Bordeaux, CNRS, Centre de Recherche Paul Pascal, CRPP, UMR 5031, 33600 Pessac, France*
[e] *Department of Inorganic Chemistry, Faculty of Science, Charles University in Prague, Hlavova 2030/8, 12843 Prague, Czech Republic*

Investigations on the spin states of octahedral Fe(II) complexes have received special attention due to their clear discrimination in the spin states of the d-orbitals. As a means to further understand the factors that influence the spin-crossover (SCO) phenomenon in Fe(II) systems, we herein report two mononuclear Fe(II) complexes, [Fe**L**$_2$]$(ClO_4)_2{\cdot}2CH_3OH$ (**1**) and [Fe**L**$_2$]$(BF_4)_2{\cdot}CH_3CN{\cdot}CH_3OH$ (**2**), derived from a novel $N_3$-donor Schiff base ligand, 2,6-bis[(3-*methylbenzylimino*)*methyl*]pyridine (**L**) with varying counteranion and the diamagnetic [Zn**L**$_2$]$(BF_4)_2$ congener for a comparative investigation. The complexes have been synthesized and characterized by electrospray-ionization mass spectrometry (ESI-MS), Fourier-transform infrared spectroscopy (FTIR), nuclear magnetic resonance (NMR) spectroscopy, single-crystal X-ray diffraction (XRD) and magnetic susceptibility studies. Structural and magnetic investigations reveal that both **1** and **2** show Fe–$N_6$ distorted octahedral geometry and are locked in the diamagnetic LS state throughout the entire explored temperature range from 1.8 to 400 K. The LS state of $[Fe\mathbf{L}_2]^{2+}$ is also confirmed by comparing the experimentally found structural parameters, NMR chemical shifts and excitation energies in the visible region with density functional theory (DFT) calculations.

## Introduction

Spin states have a major role in defining the structure, reactivity, magnetic and spectroscopic properties of coordination compounds [1–3]. The change of spin state is accompanied primarily by a change in the electronic structure of the central metal ion, which varies the physical and chemical properties of the substances [4,5]. A clear discrimination with respect to spin state is observable in the case of transition metal complexes [6], due to the nature of d-orbitals of the metals which are close in energy and can be occupied in different ways depending on the metal oxidation state, its ligand field and coordination geometry [7–9]. Transition metal complexes in various coordination geometries (e.g., octahedral, square-pyramidal, trigonal–bipyramidal, tetrahedral) [10–13] show variable spin states and the switching between can be affected by external stimuli, such as temperature, light irradiation or pressure [3,14–16]. Particularly, the spin states of mononuclear Fe(II) Schiff base complexes have been extensively studied in the view of both theory and applications [17–19]. In the case of Fe(II) ion ($3d^6$), the two possible electronic distributions among the 3d split orbitals correspond to diamagnetic (LS, S = 0) [20–23] or paramagnetic (HS, S = 2) [24–26] molecular states, which can be proved by various spectroscopic techniques and magnetic measurements. In other words, a more gradual rise of the magnetic moments with temperature is designated as a ''spin cross-over'' (SCO) situation, where the high spin and the low spin states are nearly at thermal equilibrium [6,27].

Schiff bases are condensation products of primary amines and carbonyl compounds and are capable of inducing SCO in coordination compounds [1,28,29]. The majority of SCO Schiff base complexes reported to date are Fe(II) mononuclear species [26,30–32], while some of them remain locked in the LS state [20,21]. It has been understood that ligand field [33], solvent [23], counteranion [34] and magnetic field [35] play an important role in determining the spin state of these

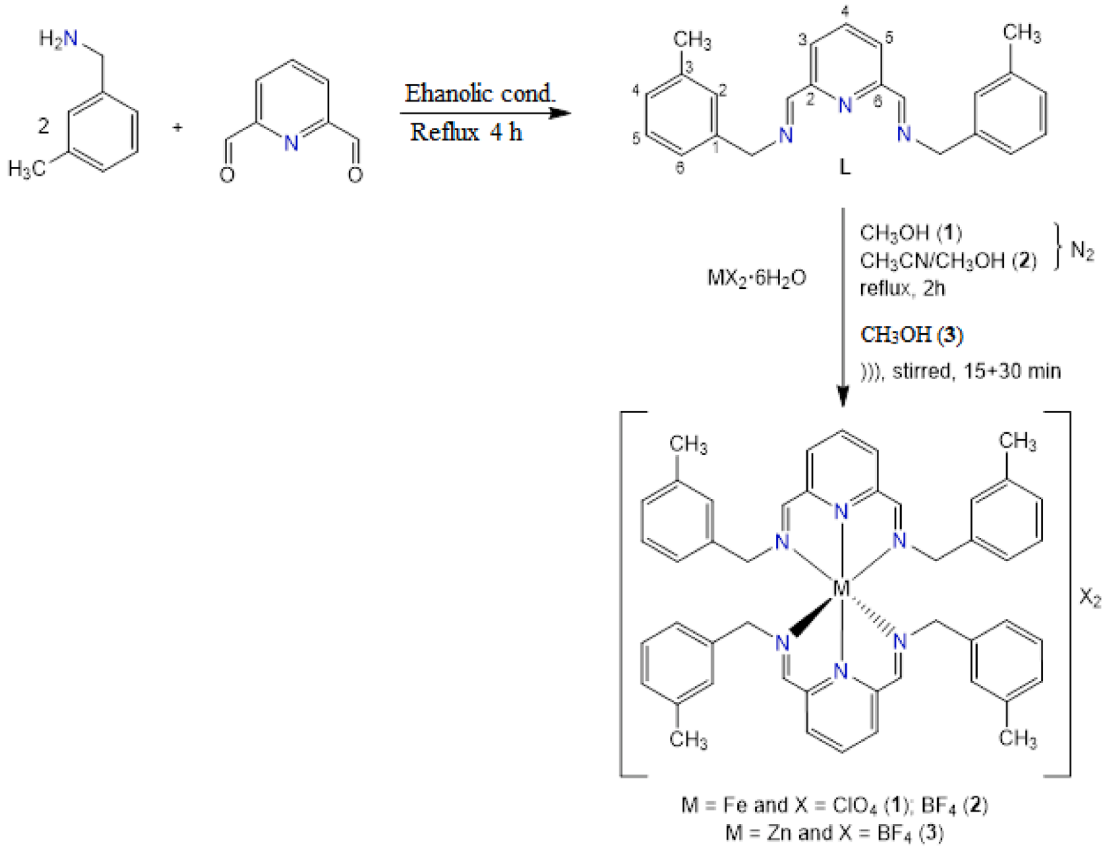


**Scheme 1.** Synthetic route for ligand **L** and complexes **1**, **2** and **3.**

complexes. Also, Fe(II) Schiff base complexes based on unsymmetrical $N_6$-coordinating ligands, either from azomethyl or pyridyl donor sites with methyl substitution, were reported to be in the LS state [21,25,34,36], because of the strong-field ligand environment pushing the complexes locked in the spin-paired condition. For acquiring the desired property using a given metal ion, it is key to tune the ligand field, which could eventually modulate the magnetic properties. In this context, Schiff bases are ideal candidates on account of their fine tunability to the ligand field by varying the substituents in both amine and aldehydic precursors.

We have shown previously, how $N_6$ coordination and substituent effects tune the SCO properties for a series of Fe(II) complexes with bis-pyrazolone pyridine ligands at room temperature [37]. In a recent review, we have also reported the effectiveness of Schiff base ligands to promote SCO in Fe(II) compounds for device-based applications [1]. In continuation of these accounts, we herein report two mononuclear Fe(II) Schiff base complexes with a $N_6$ coordination site derived from a novel Schiff base, 2,6-bis[(3-methylbenzylimino)methyl]pyridine (**L**) with varying counteranion (perchlorate and tetrafluoroborate), along with a diamagnetic Zn(II) congener for comparative studies. For all these, the structural, spectroscopic and magnetic characterization have been done, which were further supported by theoretical calculations. Although both the Fe(II) complexes remain locked in the diamagnetic state up to 400 K, the detailed investigations reported herein can be helpful in rational engineering of further molecular magnetic materials having SCO behavior with N-donor Schiff base ligands.

## Experimental

### *Materials and methods*

All chemicals were of analytical grade, used as received from the commercial sources and all complexation reactions for Fe(II) and Zn(II) were carried out under nitrogen atmosphere and ambient conditions, respectively. Single-crystal X-ray diffraction (XRD) measurements were carried out on a Bruker D8 VENTURE diffractometer equipped with a PHOTON III detector and two microfocus X-ray sources. The monochromatic primary radiation used was CuKα for **L** and MoKα for **1**, **2** and **3**. Data reduction was done using the diffractometer software. The phase problem was solved by intrinsic phasing (SHELXT) [38] and the structural models were refined by full-matrix least-squares on $F^2$ values (SHELXL) [39]. Hydrogen atoms were put into idealized positions and were refined using the riding model. NMR spectra were recorded with Bruker Ascend$^{TM}$ 400 (400 MHz for $^1$H and 101 MHz for $^{13}$C) instruments with tetramethylsilane (TMS) as an internal reference. The two-dimensional heteronuclear NMR techniques (HSQC and HMBC) were used for unambiguous assignment of chemical shifts on hydrogen and carbon atoms. FTIR spectra were measured on Agilent Technologies Cary 630 FTIR from 4000 to 400 cm$^{-1}$ range using KBr pellets. Melting points were determined on a Büchi Melting Point M−565 apparatus. Elemental analyses were carried out with FLASH elemental analyzer 1112 CHNS-O (Thermo Finnigan, Italia). The magnetic measurements were performed on a Quantum Design MPMS-XL SQUID magnetometer operating between 1.8 and 400 K and applied dc fields of up to 7 T. The measurements were performed on powder or microcrystalline samples (15–30 mg) sealed in polypropylene bags (size ~ 3 × 0.5 × 0.02 cm$^3$) under argon. The data were corrected for the intrinsic diamagnetic contributions of the sample and the sample holder. Electrospray-

ionization mass spectrometry (ESI–MS) was performed using ESI-ToF mass spectrometer (Bruker Daltonics micrOTOF-Q II).

*CAUTION. Handling with metal–organic perchlorates is potentially dangerous due to their explosive properties. It should be handled with care in small quantities.*

### Synthesis

#### Synthesis of pyridine-2,6-dicarboxaldehyde

Pyridine-2,6-dicarboxaldehyde was prepared according to the reported procedure [40] with modifications as follows. Selenium dioxide (7.98 g, 72 mmol) was added to 2,6-bis(hydroxymethyl)pyridine (10.0 g, 72 mmol) dissolved in a freshly distilled dioxane (200 mL). The reaction mixture was refluxed with stirring at 101 °C for 5 h. Subsequently, the oxide residue was separated from the solution by vacuum filtration and the light-yellow filtrate was concentrated under reduced pressure. The obtained solid was dissolved in a minimal amount of chloroform and filtered through a short pad of silica. The pale-yellow filtrate was concentrated under reduced pressure providing the desired product in 96 % yield (9.33 g). Mp. 123–125 °C. $^1$H NMR (400 MHz, $CDCl_3$) $\delta$ 10.17 (s, 2H, CHO), 8.18 (d, $J$ = 7.7 Hz, 2H, py-3,5), 8.08 (t, $J$ = 7.7 Hz, 1H, py-4) (Fig. S1). $^1$H NMR characteristics match those reported previously in [40].

#### Synthesis of the ligand, **L** ((E,E)-2,6-bis[(3-methylbenzylimino) methyl]pyridine)

The tridentate Schiff base ligand **L** was prepared by adding a solution of 3-methylbenzylamine (0.76 mL, 6.07 mmol) in ethanol (5 mL) to a stirred solution of pyridine-2,6-dicarboxaldehyde (0.41 g, 3.03 mmol) in ethanol (30 mL) (Scheme 1). The mixture was allowed to reflux for 4 h while stirring continuously. Upon cooling to 4 - 5 °C, the ligand had crystallized out of the solution and was separated as off-white crystalline product. Off-white needle-like crystals suitable for single-crystal XRD studies were obtained by slow evaporation of the solvent (~1 week) from methanolic solution of **L**. Yield: 0.5 g (48 %). Mp. = 88.1 °C. $^1$H NMR (400 MHz, $CH_3OH$-$d_4$) $\delta$ 8.52 (s, 2H, CH = N), 8.06 (d, $J$ = 7.7 Hz, 2H, py-3,5), 7.94 (t, $J$ = 7.7 Hz, 1H, py-4), 7.23 (t, $J$ = 7.5 Hz, 2H, Ar), 7.16 (s, 2H, Ar), 7.11 (m, 4H, Ar), 4.84 (s, 4H, 2 × $CH_2$), 2.33 (s, 6H, 2 × $CH_3$). $^{13}$C NMR (101 MHz, $CH_3OH$-$d_4$) $\delta$ 162.6, 153.4, 138.2, 138.0, 137.7, 128.6, 128.2, 127.6, 125.0, 122.6, 64.3, 20.0 (Figs. S2-S4). FTIR ($\bar{\nu}$, $cm^{-1}$): 3042 (w), 3002 (w), 2868 (w), 1646 (s), 1605 (m), 1585 (s), 1566 (s), 1490 (m), 1465 (s), 1411 (s), 1354 (s), 1316 (s), 1241 (m), 1219 (m), 1087 (m), 1046 (s), 993 (s), 940 (m), 904(s), 883 (s), 807 (s), 736 (s) and 692 (s).

#### Synthesis of [Fe**L**$_2$](ClO$_4$)$_2$.2CH$_3$OH (**1**)

To a stirred solution of **L** (0.34 g, 1.00 mmol) in methanol (20 mL), Fe$(ClO_4)_2$·$6H_2O$ (0.181 g, 0.5 mmol) in 3 mL of methanol was added under $N_2$ atmosphere. The color of the solution had changed to purple immediately upon mixing. The resultant purple mixture was refluxed for 2 h with continuous stirring, subsequently cooled to room temperature and filtered. Slow diffusion of diethyl ethyl into the filtrate yielded in about two weeks black block-like crystals of **1**, which were suitable for single-crystal XRD measurements. Yield: 0.2 g (42 %). $^1$H NMR (400 MHz, $CH_3OH$-$d_4$) $\delta$ 8.48 (t, $J$ = 7.8 Hz, 2H, py-4), 8.18 (d, $J$ = 7.8 Hz, 4H, py-3,5), 7.85 (s, 4H, N = CH), 7.11 (d, $J$ = 7.2 Hz, 4H, Ar), 7.01 (t, $J$ = 7.4 Hz, 4H, Ar), 6.29 (d, $J$ = 7.1 Hz, 4H, Ar), 6.22 (s, 4H, Ar), 3.74 (s, 8H, 4 × $CH_2$), 2.22 (s, 12H, 4 × $CH_3$). $^{13}$C NMR (101 MHz, $CH_3OH$-$d_4$) $\delta$ 170.1, 160.6, 138.8, 136.5, 133.1, 129.7, 128.8, 128.7, 127.7, 125.2, 62.6, 20.4 (Figs. S5-S7). FTIR ($\bar{\nu}$, $cm^{-1}$): 3002 (w), 2921 (w), 2885 (w), 1607 (s), 1589 (s), 1532 (s), 1489 (s), 1446 (s), 1400 (s), 1368 (s), 1207 (m), 1168 (m), 1073 (s), 967 (m), 937 (m), 896 (m), 785 (s), 750 (s), 706 (s), 680 (m), 620 (s), 456 (s) and 430 (s). ESI-MS: $m/z$ for $FeC_{46}H_{46}N_6$ $[M]^{2+}$: 369.1562. Found: 369.1623. $m/z$ for $FeC_{46}H_{46}N_6ClO_4$ $[M-ClO_4]^+$: 837.2614. Found: 837.2165.

#### Synthesis of [Fe**L**$_2$](BF$_4$)$_2$·CH$_3$CN·CH$_3$OH (**2**)

$Fe(BF_4)_2$·$6H_2O$ (0.17 g, 0.50 mmol) was added to a well-stirred solution of **L** (0.34 g, 1.00 mmol) in a mixture of acetonitrile/methanol (20 mL, 1:1) under $N_2$ atmosphere. Upon the addition of the metal salt, a purple color developed for the resultant solution. The mixture was refluxed for 2 h under continuous stirring and subsequently allowed to cool to room temperature and filtered. Black block-shaped crystals appropriate for single-crystal XRD measurements were produced by the slow diffusion of diethyl ether into the filtered solution. Yield: 0.23 g (46 %). $^1$H and $^{13}$C NMR characteristics of **2** are identical with those of **1** reported above (Figs. S5-S7). FTIR ($\bar{\nu}$, $cm^{-1}$): 3026 (w) 2902 (w), 1607 (s), 1528 (s), 1489 (s), 1448 (m), 1397 (s), 1373 (m), 1339 (m), 1284 (m), 1208 (m), 1167 (s), 1031 (s), 997 (w), 787 (s), 750 (s), 737 (s), 703 (s), 681 (s), 631 (m), 520 (s) and 456 (s). ESI-MS: $m/z$ for $FeC_{46}H_{46}N_6$ $[M]^{2+}$: 369.1751. Found: 369.1562. $m/z$ for $FeC_{46}H_{46}N_6ClO_4$ $[M-BF_4]^+$: 837.2614. Found: 837.2165.

#### Synthesis of [Zn**L**$_2$](BF$_4$)$_2$ (**3**)

Ligand **L** (0.15 g, 0.44 mmol) and $Zn(BF_4)_2$·$6H_2O$ (0.076 g, 0.22 mmol) were mixed in methanol (4 mL), the mixture was sonicated for 15 min and then stirred at room temperature for 30 min. The precipitated white solid was filtered, washed with diethyl ether and dried under vacuum, affording **3** in 72 % yield (0.146 g). Slow diffusion of diethyl ether into the methanolic/chloroform solution of **3** afforded grey needle-like crystals were obtained, which were suitable for single-crystal XRD measurements. FTIR ($\bar{\nu}$, $cm^{-1}$): 3080 (w) 2918 (w), 1643 (s), 1580 (s), 1488 (s), 1471 (m), 1437 (m), 1307 (s), 1333 (m), 1221 (m), 1207 (m), 1168 (s), 1032 (s), 880 (m), 789 (s), 747 (s), 706 (s), 678 (s), 659 (m), 628 (m), 518 (s) and 458 (s). $^1$H NMR (400 MHz, $CH_3OH$-$d_4$) $\delta$ 8.58 (t, $J$ = 7.8 Hz, 2H, py-4), 8.18 (s, 4H, N = CH), 8.02 (d, $J$ = 7.8 Hz, 4H, py-3,5), 7.06 (d, $J$ = 7.2 Hz, 4H, Ar), 6.92 (t, $J$ = 7.4 Hz, 4H, Ar), 6.44 (s, 4H, Ar), 6.40 (d, $J$ = 7.1 Hz, 4H, Ar), 4.26 (s, 8H, 4 × CH2), 2.14 (s, 12H, 4 × CH3). $^{13}$C NMR (101 MHz, $CH_3OH$-$d_4$) $\delta$ 159.3, 146.0, 144.1, 138.1, 134.8, 129.7, 129.0, 128.9, 128.4, 125.5, 61.4, 20.0 (Figs. S8-S9).

### Computational details

The structures of all systems under investigation were fully optimized (without counterion) in Turbomole [41] at the TPSSh level of theory, [42] including an atom-pairwise correction for dispersion forces (Grimme's D3 model) with Becke-Johnson (BJ) damping [43,44] and employing def2-TZVP basis set for all atoms [45]. The optimized structures were characterized as true minima on the potential energy hypersurface by harmonic vibrational frequency analyses. Calculations of NMR nuclear shieldings were performed in the Gaussian 16 program package [46] using gauge-including atomic orbitals (GIAO) at the same level as structure optimization (TPSSh-D3(BJ)/def2-TZVP). In these calculations, bulk solvent effects were simulated by means of the integral equation formalism of the polarizable continuum model (IEF-PCM) [47]. The calculated shieldings were converted to chemical shifts (δ in ppm) relative to the shieldings of tetramethylsilane (TMS). Time-dependent DFT calculations of excitation energies were performed using the Gaussian 16 code at the same level as NMR shielding calculations (TPSSh-D3(BJ)/def2-TZVP/PCM).

### Synthesis of Schiff base **L**, complexes **1**, **2** and **3** and spectroscopic investigation of their electronic structure

The synthesis of the ligand **L** was based on the condensation of 3-methylbenzylamine with pyridine-2,6-dicarboxaldehyde upon refluxing in ethanol (Scheme 1). Crystals of **L** suitable for single-crystal XRD studies were grown by slow evaporation of the solvent from a methanolic solution of the ligand at room temperature. In the IR spectrum of **L**, the disappearance of the strong aldehydic carbonyl absorption band

**Table 1**
Experimental $^{1}$H NMR chemical shifts (in ppm vs TMS) for the free ligand **L** and corresponding $[Fe(\mathbf{L})_2]^{2+}$ and $[Zn(\mathbf{L})_2]^{2+}$ complexes (all measured in $CH_3OH$-$d_4$) [a].

| | H-imine | py-3,5 | py-4 | $CH_2$ | H-2 | H-4 | H-5 | H-6 | $CH_3$ |
|---|---|---|---|---|---|---|---|---|---|
| **L** | 8.52 | 8.06 | 7.94 | 4.84 | 7.16 | 7.09 | 7.23 | 7.12 | 2.33 |
| $[Fe(\mathbf{L})_2]^{2+}$ | 7.85 | 8.18 | 8.49 | 3.74 | 6.22 | 7.11 | 7.01 | 6.29 | 2.22 |
| $[Zn(\mathbf{L})_2]^{2+}$ | 8.18 | 8.03 | 8.58 | 4.26 | 6.44 | 7.06 | 6.92 | 6.40 | 2.14 |
| $\Delta\delta(^{1}H)_{Fe,L}$ [b] | −0.67 | +0.12 | +0.55 | −1.10 | −0.94 | +0.02 | −0.22 | −0.83 | −0.11 |
| $\Delta\delta(^{1}H)_{Fe,Zn}$ [c] | −0.33 | +0.15 | −0.09 | −0.52 | −0.22 | +0.05 | +0.09 | −0.11 | +0.08 |

[a] See SI for corresponding experimental NMR spectra and computed chemical shifts. [b] $^{1}$H NMR coordination shifts as a difference between resonance of given $^{1}$H nuclei in the Fe(II) complex and the free ligand. [c] Difference in $^{1}$H NMR resonances of given $^{1}$H nuclei in the Fe(II) and Zn(II) complex.

**Table 2**
Experimental $^{13}$C NMR chemical shifts (in ppm vs TMS) for the free ligand **L** and corresponding $[Fe(\mathbf{L})_2]^{2+}$ and $[Zn(\mathbf{L})_2]^{2+}$ complexes (all measured in $CH_3OH$-$d_4$) [a].

| | C-imine | py-2,6 | py-3,5 | py-4 | $CH_2$ | C-1 | C-2 | C-3 | C-4 | C-5 | C-6 | $CH_3$ |
|---|---|---|---|---|---|---|---|---|---|---|---|---|
| **L** | 162.6 | 154.0 | 122.6 | 137.7 | 64.3 | 138.2 | 128.6 | 138.1 | 127.6 | 128.2 | 125.0 | 20.0 |
| $[Fe(\mathbf{L})_2]^{2+}$ | 170.1 | 160.6 | 127.7 | 136.5 | 62.6 | 133.1 | 128.8 | 138.8 | 129.7 | 128.7 | 125.2 | 20.4 |
| $[Zn(\mathbf{L})_2]^{2+}$ | 159.3 | 144.1 | 129.7 | 146.0 | 61.4 | 134.8 | 129.0 | 138.1 | 129.0 | 128.4 | 125.5 | 20.0 |
| $\Delta\delta(^{13}C)_{Fe,L}$ [b] | +7.5 | +6.6 | +5.1 | −1.2 | −1.7 | −5.1 | +0.2 | +0.7 | +2.1 | +0.5 | +0.2 | +0.4 |
| $\Delta\delta(^{13}C)_{Fe,Zn}$ [c] | +10.8 | +16.5 | −2.0 | −9.5 | +1.2 | −1.7 | −0.2 | +0.7 | +0.7 | +0.3 | −0.3 | +0.4 |

[a] See SI for corresponding NMR spectra and computed chemical shifts. [b] $^{13}$C NMR coordination shifts as a difference between resonance of given $^{13}$C nuclei in the Fe (II) complex and the free ligand. [c] Difference in $^{1}$H NMR resonances of given $^{1}$H nuclei in the Fe(II) and Zn(II) complex.

and the appearance of new bands at 1646 and 1585 cm$^{-1}$, respectively, corresponds to the azomethine and pyridyl C=N groups, which confirms the formation of the desired Schiff base ligand. The $^{1}$H and $^{13}$C NMR spectra of **L** exhibit key resonances at 8.52 and 162.6 ppm, respectively, assigned to the azomethine group (Figs. S2–S4). $^{1}$H and $^{13}$C NMR resonances of pyridine moiety are observed between 8.06 and 7.94 and 154.0–122.6 ppm, respectively (see Tables 1 and 2 for more detailed assignments and Tables S2–S3 in the Supplementary Information for DFT computed NMR chemical shifts).

Complexes **1** and **2** were synthesized by the stoichiometric reaction (1:2) of the iron(II) salt ($Fe(ClO_4)_2{\cdot}6H_2O$ in methanol or $Fe(BF_4)_2{\cdot}6H_2O$ in a mixture acetonitrile/methanol) with **L** (Scheme 1). Additionally, the diamagnetic congener **3** was prepared analogously using $Zn(BF_4)_2{\cdot}6H_2O$ in THF. In the case of **1** and **2**, the reactions were performed under inert atmosphere, while **3** was synthesized under ambient conditions. After the completion of the reactions, black block-like crystals were obtained for **1** and **2**, whereas grey needle-shaped crystals were formed for **3**. The infrared spectra of **1**, **2** and **3** showed characteristic bands at 1607 and 1532 cm$^{-1}$ for **1**, 1607 and 1528 cm$^{-1}$ for **2** and 1643 and 1580 cm$^{-1}$ for **3** corresponding to the azomethine and pyridyl C=N stretching vibrations [24,48,49]. The ESI-MS data are also in conformity with the assigned molecular formulae (Fig. S10).

Since the different counteranions in **1** and **2** have practically no impact on the observed NMR resonances, because of the dissociation of ion-pairs in solution, we have taken only **2** as a phototype and compared it with the Zn(II) analogue **3**. Coordination of **L** with Fe(II) in **2** shifts the imine $^{1}$H NMR peaks towards lower resonance frequencies by 0.67 ppm, while the imine carbons are deshielded to 170.1 ppm, thus by about + 7.5 ppm. Even larger $^{1}$H shielding effects upon Fe(II) complexation are observed for the benzylic $CH_2$ groups ($\Delta\delta(^{1}H)_{Fe,L}$ = ca. −1.1 ppm) and *ortho*-hydrogens ($\Delta\delta(^{1}H)_{Fe,L}$ = -0.94 ppm). On the contrary, the largest coordination-induced $^{1}$H deshielding ($\Delta\delta(^{1}H)_{Fe,L}$ = +0.55 ppm) is seen for a hydrogen atom of the pyridine moiety at the position 4 (py-4). Apart from the imine carbons, the coordination-induced $^{13}$C deshieldings are observed also for pyridine-2/-6 and pyridine-3/-5 carbons, while benzylic C-1 carbons on the phenyl ring experience the most pronounced coordination-induced $^{13}$C shielding ($\Delta\delta(^{13}C)_{Fe,L}$ = -5.1 ppm).

The $^{1}$H NMR resonances in Fe(II) complex **2** resemble those of the diamagnetic Zn(II) congener (**3**) with only minor shielding/deshielding effects (Figs. S5 and S8). The most pronounced effect is found for the benzylic $CH_2$ group, which is somewhat more shielded in Fe(II) species and the reordering of the chemical shifts (e.g. imine CH = N hydrogen in Zn(II) is more deshielded than pyridine-3,5 hydrogens, thus opposite as found in Fe(II) complexes). Additionally, the imine and pyridine-2,6 $^{13}$C resonances in Fe(II) complexes are deshielded by more than 10 ppm compared to their Zn(II) congener (Figs. S6 and S9). These notably different NMR coordination shifts coincide qualitatively with DFT calculations and can be attributed to the shorter iron-ligand contacts ($d(Fe–N_{py})_{av}$ = 1.881 Å; $d(Fe–N_{imine})_{av}$ = 1.983 Å) as compared to those in Zn(II) congener ($d(Zn–N_{py})_{avrgd}$ = 2.083 Å; $d(Zn–N_{imine})_{avrgd}$ = 2.240 Å) as well as to the larger Fe(II)-N bond covalency and the off-center paramagnetic ring currents in the vicinity of Fe(II) center with the partially-filled $d^6$ shell [50–54] (see also Table S4).

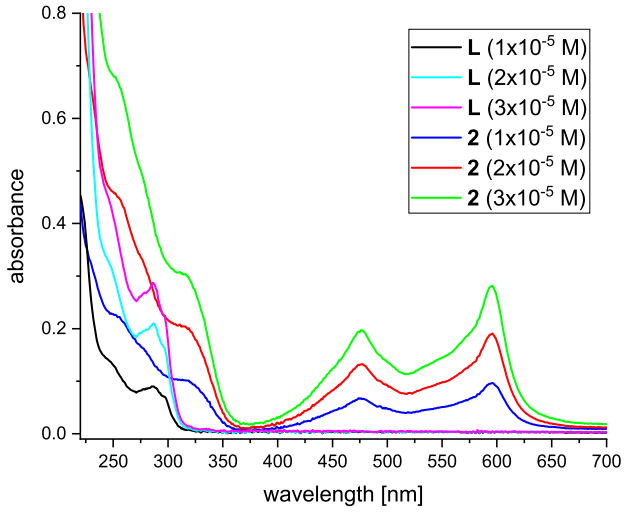


**Fig. 1.** UV–vis absorption spectra of the free ligand (**L**) and Fe(II) complex **2** in acetonitrile at three different concentrations.

The Fe(II) complex **2** shows notable UV–visible absorption peaks positioned in the visible region at 595 and 476 nm (see Fig. 1), which is linked to the deep purple color of these complexes in acetonitrile solution. These absorption bands match very well with those computed by means of time-dependent DFT ($E_1$ = 610 nm, $f_{osc}$ = 0.009, the dominant transitions: HOMO → LUMO and HOMO → LUMO + 1 and $E_5$ = 498 nm, $f_{osc}$ = 0.018, the dominant transitions: HOMO-2 → LUMO and HOMO-1 → LUMO + 1) and are attributed to the metal-to-ligand charge-transfer (MLCT) from Fe(II) ion to pyridine and imine moieties (see Fig. 2 for

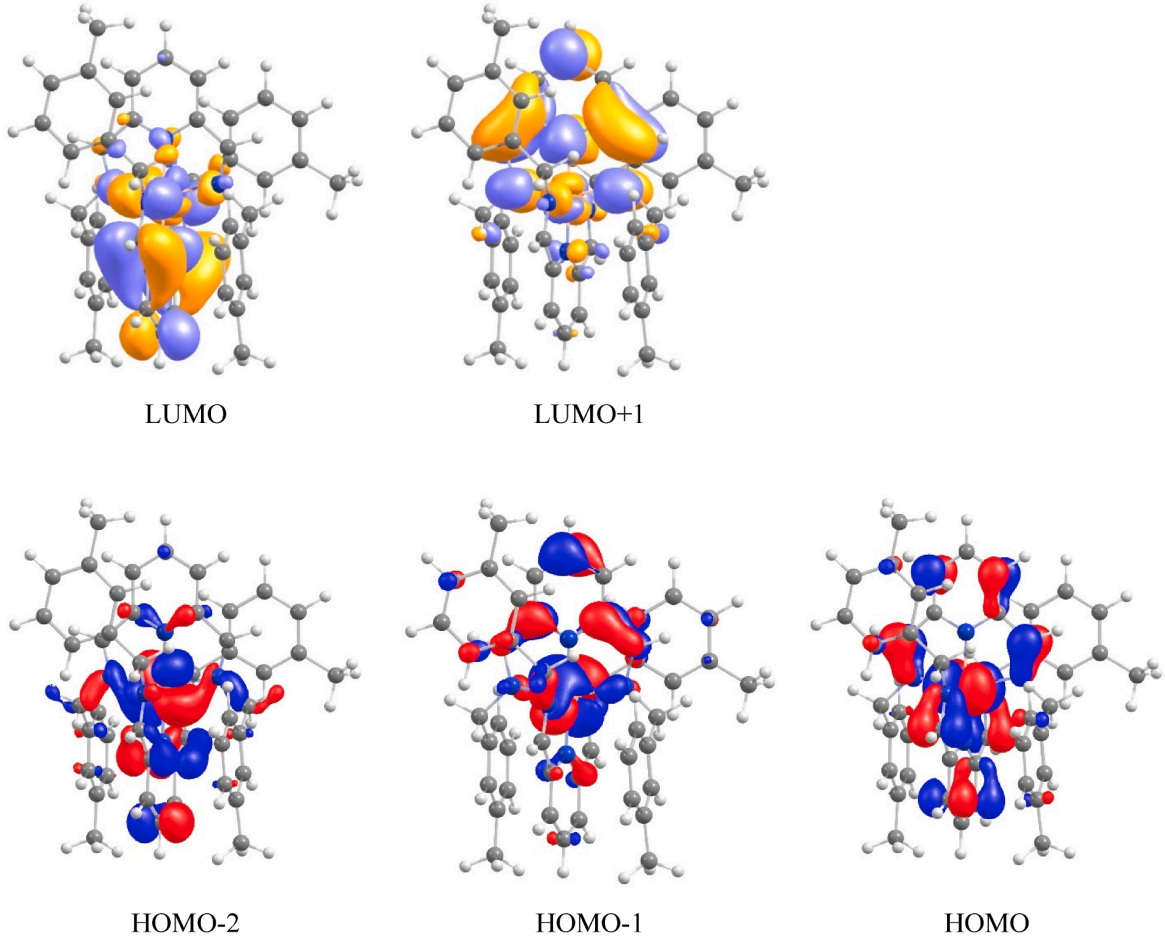


**Fig. 2.** DFT calculated frontier molecular orbitals in $[Fe(\mathbf{L})_2]^{2+}$ involved in electronic transitions in the visible region.

corresponding frontier molecular orbitals involved in these electronic transitions).

*Single-crystal X-ray diffraction analysis*

Single crystals of the ligand, **L** suitable for X-ray crystal structure analysis were grown from a methanolic solution at room temperature upon slow evaporation of the solvent. **L** crystallizes in the monoclinic space group $P2_1/c$ with $Z = 4$. The N-C bond distances are in the range 1.3434(12)–1.4604(12) Å with an average value of 1.4075(12) Å. Selected crystallographic data, bond distances and angles of the ligand are shown in Table 3, Fig. 3 and Table S1.

Structural analysis of the XRD data reveals that the asymmetric unit of **1** consists of one $[FeL_2]^{2+}$ cation, two $ClO_4^-$ anions and two methanol molecules (Fig. 4a), whereas for **2**, one $[FeL_2]^{2+}$ cation, two $BF_4^-$ anions as well as a molecule of both acetonitrile and methanol are present (Fig. 4b). Also, **3** consist of one $[ZnL_2]^{2+}$ cation and two $BF_4^-$ anions without the presence of solvent in the lattice. Selected bond lengths and angles are summarized in Table 4. The packing of the unit cell for both **1** and **2** consists of two complex units, four counteranions and four solvent molecules (Fig. S11b-c). Whereas the packing of **3** consists of two complex units and four counteranions (Fig. S11d).

The Fe(II) and Zn(II) centers are coordinated to six nitrogen donor atoms of two ligand moieties and adopt a distorted octahedral geometry. The two pyridyl nitrogen atoms of the ligand occupy the axial positions and the four imino nitrogen atoms occupy the equatorial plane (Fig. 4). The Fe–N bond distances are in the range 1.868(2)–1.994(2) Å for **1** and 1.860(6)–2.003(6) Å for **2**. Moreover, the average $Fe–N_{pyridine}$ and $Fe–N_{imino}$ bond distances are 1.869(2) and 1.98575(2) Å for **1,** and 1.8655(6) and 1.9855(6) Å for **2**, respectively (Table 4). These distances observed are typical for LS Fe(II), within the range of reported Fe(II) − N bond lengths (e.g., 1.88 to 2.06 Å) in mononuclear SCO complexes [22,23]. This hypothesis is also confirmed by the magnetic investigations [33,55,56]. The axially coordinated pyridyl nitrogen atoms are almost linear with N(2)–Fe(1)–N(5) angle of 178.25(10)° for **1** and 177.9(3)° for **2** (Table 4) [57,58]. For the Zn(II) congener, the average Zn–N bond distance is 2.179 Å) and the average $Zn–N_{pyridine}$ and $Zn–N_{imino}$ bond distances are 2.2425 and 2.052 Å (Table 4).

Looking at the intermolecular interactions within the molecular packing of **1**, π-π interaction exist through phenyl rings of the ligands in the *ab*-plane (Fig. S11a) along with a weak hydrogen bonding interaction between the oxygen atom of perchlorate counteranion and hydrogen atom of methanol, with O7···H9O distance of 2.04(6) Å and maximum D-A ($ClO_4^-$···H(methanol)) distance of 2.9(6) Å and minimum angle of 120° for **1** (Fig. S11b). However, there is no π-π interaction as well as hydrogen bonding in **2**. Hydrogen bonding and π-π interactions that are mediated by counterions, in the present cases, have negligible effect on the spin state of the metal centers, thereby remain, both in the diamagnetic condition (*vide infra*) [59,60]. Also, molecular packing of **1** shows weak intermolecular short contacts with an average distance of 2.61864(5) Å and for **2,** short contacts exist with an average distance of 2.6711(2) Å (Fig. S11c) [61].

**Table 3**
Crystallographic data and selected data collection parameters for compounds **L**, **1**, **2** and **3.**

| Parameters | L | 1 | 2 | 3 |
|---|---|---|---|---|
| Sum formula | $C_{23}H_{23}N_3$ | $C_{48}H_{54}Cl_2FeN_6O_{10}$ | $C_{49}H_{53}B_2F_8FeN_7O$ | $C_{46}H_{45}B_2ZnF_6N_6$ |
| FW (g/mol) | 341.44 | 1001.72 | 985.45 | 877.46 |
| Cell volume (Å$^3$) | 1839.4(3) | 2325.25(16) | 2305.3(20) | 2440.4(5) |
| Space group | $P2_1/c$ | *P*-1 | *P*-1 | *Pn* |
| Crystal system | Monoclinic | Triclinic | Triclinic | Monoclinic, |
| Temperature (K) | 120(2) | | | |
| Density (g cm$^{-3}$) | 1.233 | 1.431 | 1.420 | 1.194 |
| *Z* | 4 | 2 | 2 | 2 |
| *a* (Å) | 19.4228(16) | 10.1438(4) | 9.9737(6) | 10.6167(12) |
| *b* (Å) | 6.1674(5) | 10.2131(4) | 10.1473(6) | 10.6216(12) |
| *c* (Å) | 15.5735(13) | 22.7248(9) | 23.0147(15) | 22.062(2) |
| *α* (°) | 90 | 87.447(1) | 88.090(2) | 90 |
| *β* (°) | 99.595(2) | 81.362(1) | 82.061(2) | 101.215(4) |
| *γ* (°) | 90 | 89.806(1) | 88.739(2) | 90 |
| Limiting indices | $-24 \le h \le 24$<br>$-7 \le k \le 7$<br>$-19 \le l \le 19$ | $-11 \le h \le 13$<br>$-13 \le k \le 13$<br>$-29 \le l \le 29$ | $-12 \le h \le 12$<br>$-12 \le k \le 12$<br>$-7 \le l \le 28$ | $-13 \le h \le 13$<br>$-13 \le k \le 13$<br>$27 \le l \le 27$ |
| Absorption coefficient (mm$^{-1}$) | 0.566 | 0.505 | 0.406 | 0.562 |
| *θ* range for data collection (°) | 5.762 to 74.503 | 2.156 to 27.527 | 2.008 to 25.999 | 2.687 to 26.013 |
| Reflections collected/ unique | 27,767 / 3750<br>[$R_{int} = 0.0276$] | 38,848 / 10,560<br>[$R_{int} = 0.0366$] | 9073 / 9073<br>[$R_{int} = 0.052$] | 58,233 / 9553<br>[$R_{int} = 0.0491$] |
| Max and min. transmission | 0.93 and 0.76 | 0.94 and 0.84 | 0.95 and 0.77 | 0.91 and 0.85 |
| Data/restraints/ parameters | 3750 / 0 / 237 | 10,560 / 0 / 688 | 9073 / 1 / 626 | 9553 / 34 / 542 |
| Goodness-of-fit on $F^2$ | 1.037 | 1.106 | 1.128 | 1.022 |
| Final *R* indices<br>[*I* greater than 2$\sigma$(*I*)] | $R_1 = 0.0396$<br>w$R_2 = 0.1103$ | $R_1 = 0.0596$<br>w$R_2 = 0.1272$ | $R_1 = 0.1085$<br>w$R_2 = 0.2605$ | R1 = 0.0722<br>w*R*2 = 0.1969 |
| *R* indices (all data) | $R_1 = 0.0406$<br>w$R_2 = 0.1114$ | $R_1 = 0.0741$<br>w$R_2 = 0.1344$ | $R_1 = 0.1225$<br>w$R_2 = 0.2669$ | R1 = 0.0787<br>w*R*2 = 0.2042 |
| Largest diff. peak and hole | 0.295 and<br>−0.243 e.Å$^{-3}$ | 1.073 and<br>−0.907 e.Å$^{-3}$ | 0.781 and<br>−0.837 e.Å$^{-3}$ | 1.173 and<br>−0.703 |
| Spin state | – | LS | LS | – |
| CCDC number | 2,151,347 | 2,128,829 | 2,128,828 | 2,193,161 |

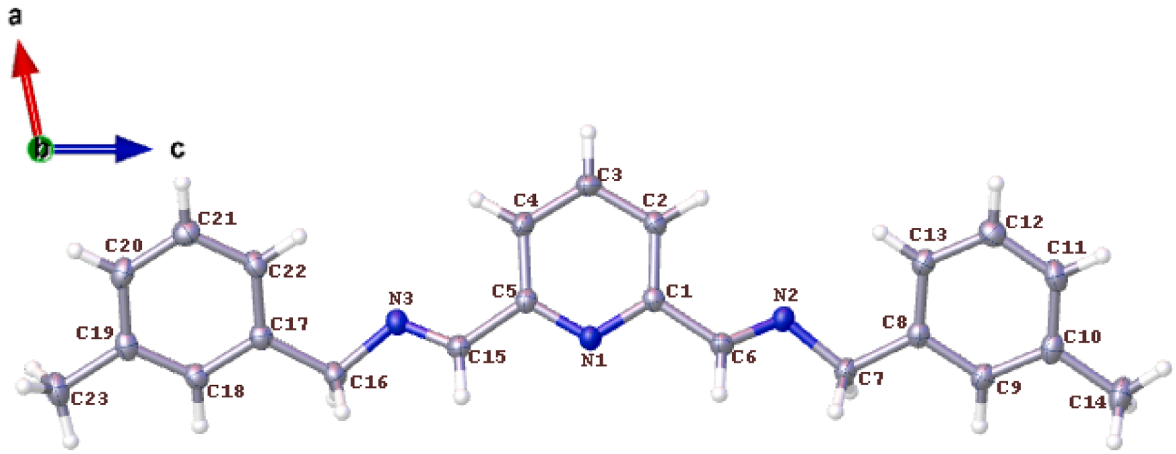


**Fig. 3.** Labelled ORTEP drawing in *b*-axis (30 % thermal ellipsoids; except for the hydrogens shown in simple ball and stick representation) of the asymmetric unit in b-axis from the crystal structure of **L** at 120 K.

*Magnetic properties and their discussion together with the DFT calculations*

The magnetic susceptibility measurements of $[FeL_2](ClO_4)_2{\cdot}2CH_3OH$ (**1**) and $[FeL_2](BF_4)_2{\cdot}CH_3CN{\cdot}CH_3OH$ (**2**) were performed for both heating (↑) and cooling cycles (↓) in the temperature range 1.8–400 K and also by varying the direct current (*dc*) field (1000 and 10,000 Oe; Figs. (S12a–b). Th $\chi T$ versus *T* plots of **1** and **2** in the whole temperature range confirm that both the compounds are locked in the diamagnetic LS state ($S = 0$) of Fe(II) $d^6$ configuration. This is in accordance with the average Fe–N bond distance observed, 1.94683(2) for **1** and 1.9455(6) Å for **2**, which is characteristic of Fe(II) in low-spin state [4]. Annealing of both compounds at 400 K did not show any change in the spin state proving that neither counterions nor lattice solvent molecules have effect on SCO nature in the present case [20]. Diamagnetic nature of both Fe(II) complexes is also supported in solution by characteristic, well-resolved $^1H$ and $^{13}C$ NMR peaks, with chemical shifts in excellent accord with those computed at the TPSSh-D3(BJ)/def2-TZVP level for closed-shell ($S = 0$) species (see Tables S2-S3 and Fig. S13 in Supplementary Information). High-spin $[Fe(L)_2]^{2+}$ complex in quintet ($S = 2$) state is computed at the same level to be energetically disfavored by 74.3 kJ/mol. This relatively large energy gap can explain the locking of

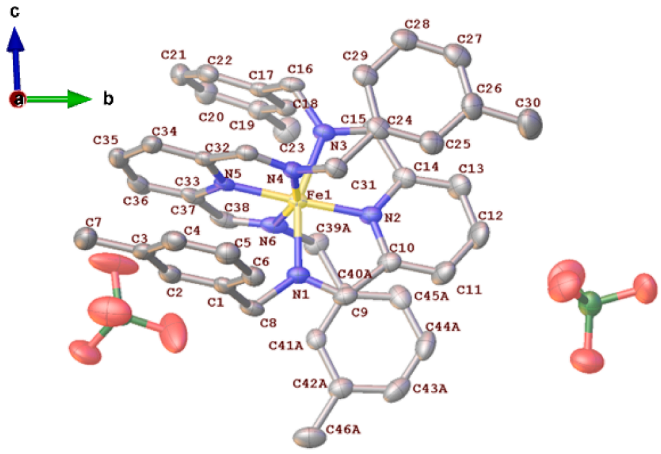


(a)

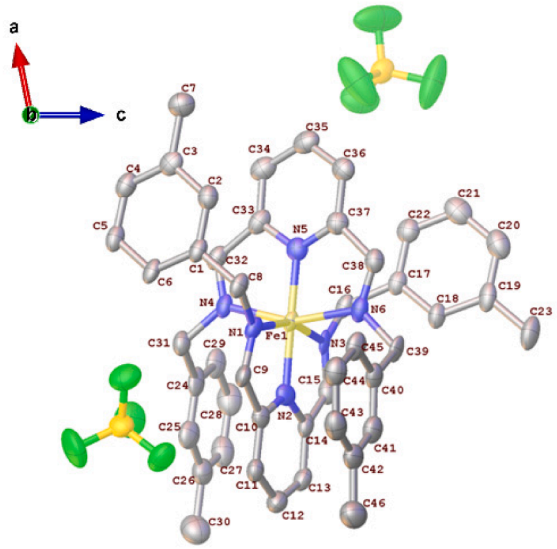


(b)

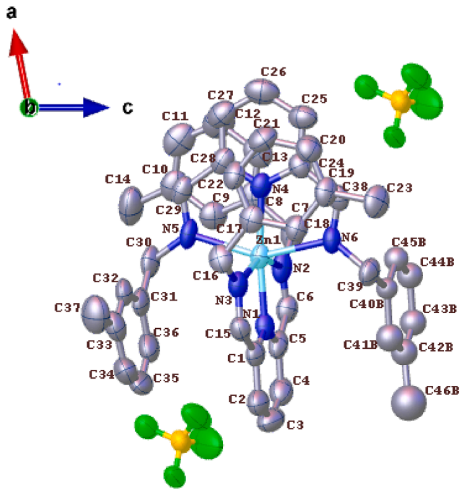


(c)

**Fig. 4.** Labelled ORTEP drawing of **1** (a) in *a*- axis and **2** (b) and **3** (c) in *b*-axis at 120 K. Thermal ellipsoids are drawn on 30 % probability level. Hydrogen atoms and solvent molecules are omitted for clarity.

**Table 4**
Selected bond lengths (Å) and angles (°) for **1**, **2** and **3** from single-crystal XRD data collected at 120 K.

| Parameter | 1 | 2 | 3 |
|---|---|---|---|
| Fe(1)–N(1) | 1.989(2) | 2.003(6) | |
| Fe(1)–N(2) | 1.870(2) | 1.871(6) | |
| Fe(1)–N(3) | 1.971(2) | 1.968(5) | |
| Fe(1)–N(4) | 1.989(2) | 1.978(6) | |
| Fe(1)–N(5) | 1.868(2) | 1.860(6) | |
| Fe(1)–N(6) | 1.994(2) | 1.993(6) | |
| Av. Fe–N | 1.94683(2) | 1.9455(6) | |
| N(2)-Fe(1)-N(5) | 178.25(10) | 177.9(3) | |
| N(1)-Fe(1)-N(3) | 159.55(10) | 159.5(3) | |
| N(4)-Fe(1)-N(6) | 159.43(11) | 159.3(3) | |
| N(1)-Fe(1)-N(5) | 101.71(10) | 102.4(2) | |
| N(2)-Fe(1)-N(6) | 100.97(11) | 100.7(3) | |
| N(2)-Fe(1)-N(4) | 99.59(10) | 100.0(3) | |
| N(3)-Fe(1)-N(5) | 98.73(10) | 98.0(3) | |
| N(1)-Fe(1)-N(6) | 92.11(9) | 92.1(2) | |
| N(3)-Fe(1)-N(6) | 92.03(10) | 92.4(2) | |
| N(1)-Fe(1)-N(4) | 91.93(9) | 91.6(2) | |
| N(3)-Fe(1)-N(4) | 91.19(9) | 91.2(2) | |
| N(1)-Fe(1)-N(2) | 79.86(10) | 79.6(3) | |
| N(5)-Fe(1)-N(6) | 79.79(10) | 79.4(3) | |
| N(2)-Fe(1)-N(3) | 79.70(10) | 79.9(3) | |
| N(4)-Fe(1)-N(5) | 79.63(10) | 79.8(3) | |
| Zn(1)-N(1) | | | 2.042(8) |
| Zn(1)-N(4) | | | 2.064(7) |
| Zn(1)-N(6) | | | 2.235(5) |
| Zn(1)-N(5) | | | 2.236(6) |
| Zn(1)-N(3) | | | 2.237(6) |
| Zn(1)-N(2) | | | 2.262(6) |
| Av. Zn–N | | | 2.179 |
| N(1)-Zn(1)-N(4) | | | 175.0(3) |
| N(1)-Zn(1)-N(6) | | | 100.2(2) |
| N(4)-Zn(1)-N(6) | | | 74.8(3) |
| N(1)-Zn(1)-N(5) | | | 109.2(3) |
| N(4)-Zn(1)-N(5) | | | 75.7(3) |
| N(6)-Zn(1)-N(5) | | | 150.6(2) |
| N(1)-Zn(1)-N(3) | | | 75.3(2) |
| N(4)-Zn(1)-N(3) | | | 105.3(2) |
| N(6)-Zn(1)-N(3) | | | 94.5(2) |
| N(5)-Zn(1)-N(3) | | | 93.9(2) |
| N(1)-Zn(1)-N(2) | | | 75.2(3) |
| N(4)-Zn(1)-N(2) | | | 104.3(3) |
| N(6)-Zn(1)-N(2) | | | 92.9(2) |
| N(5)-Zn(1)-N(2) | | | 93.5(2) |
| N(3)-Zn(1)-N(2) | | | 150.5(3) |

the spin-states of these complexes in the closed-shell state ($S = 0$) over a wide temperature range. The similar spin-paired, low spin state has been observed in previous reports, where $N_6$ coordination occurred in octahedral Fe(II) Schiff base complexes [21–23]. From these reports, coordination of four azomethine and two pyridyl nitrogens to the Fe(II) centers locked the complexes in the low spin state, due to the strong ligand field [22]. Conversely, octahedral coordination occupied by pyridyl [24], imidazolo [25,26] and tetrazolo [62] nitrogen coordination induce weaker ligand field, favoring high spin condition, leading SCO nature. Similar properties were observed by Wang and co-workers in six-coordinate Fe(II) complexes with $N_6$coordination environment, having a methyl substituted pyridylimine based Schiff base complex [23].

## Conclusions

We have synthesized and characterized two Fe(II) mononuclear complexes **1** and **2** based on $N_3$-donor Schiff base ligand, **L** by varying counteranions, such as perchlorate and tetrafluoroborate and compared with diamagnetic zinc analogue. Single-crystal XRD investigations reveal that, both the complexes have a distorted octahedral coordination geometry in which each metal center is bounded by six nitrogen donors from two ligand motifs (four azomethine N and two pyridyl N). Both compounds are isostructural with two complex units per unit cell, four solvent molecules and four counteranions. Magnetic susceptibility measurements revealed that the spin-state of both compounds remain in the diamagnetic state throughout the measured temperature range 1.8–400 K. Annealing of both complexes at 400 K led to the loss of the solvent molecules from the lattice but they remain LS. The type of counteranion ($ClO_4^-$ or $BF_4^-$) and solvents (acetonitrile or methanol) did not change their spin-states.The reported results appear to be particularly important for further design of SCO materials and give a right direction to synthesize new Fe(II) Schiff base SCO systems. Further investigations by varying the ligand field, introducing substitutions in the ligand moiety are under way.

This research project was supported by the National Scholarship Programme of the Slovak Republic 2021 and Addis Ababa Science and Technology University, Addis Ababa, Ethiopia. This work was also supported by the Slovak Research and Development Agency (Grant No. APVV-21–0503) and the Grant Agency of the Ministry of Education of the Slovak Republic (VEGA Project No. 1/0669/22).

We are thankful to National Scholarship Programme of the Slovak Republic 2021 for a research stay and Woldia University, Ethiopia for a Ph.D. studentship to Y.B. We are also thankful to the University of Bordeaux, the Région Nouvelle Aquitaine, Quantum Matter Bordeaux (QMBx), the Centre National de la Recherche Scientifique (CNRS), and the Association Française de Magnétisme Moléculaire. We would like to thank Prof. Jozef Noga from Comenius University in Bratislava for his keen interest and support during this work. Mr. Tesfay Gebretsadik from Changchun Institute of Applied Chemistry, CAS, China is thankfully acknowledged for his support during this work.

[1] K. Senthil Kumar, Y. Bayeh, T. Gebretsadik, F. Elemo, M. Gebrezgiabher, M. Thomas, M. Ruben, Dalt. Trans. 48 (2019) 15321–15337.
[2] M.A. Halcrow, Crystals. 6 (2016) 58.
[3] B. Brachňaková, J.A. Kožíšková, J. Kožíšek, E. Melníková, M. Gál, R. Herchel, T. Dubaj, I. Šalitroš, Dalt. Trans. 49 (2020) 17786–17795.
[4] M.A. Halcrow, Polyhedron 26 (2007) 3523–3576.
[5] H.J. Shepherd, C.M. Quintero, S. Tricard, L. Salmon, A. Bousseksou, Nat. Commun. 4 (2013).
[6] P. Gütlich, A.B. Gaspar, Y. Garcia, Beilstein J. Org. Chem. 9 (2013) 342–391.
[7] O. Kahn. Molecular magnetism, VCH Publishers, Inc, New York, 1993.
[8] J. Olguín, S. Brooker, Spin-Crossover in Discrete Polynuclear Complexes: Spin-Crossover Materials: Properties and Applications, Willey (2013) 77–120.
[9] A. Hauser, Adv Polym Sci. 233 (2004) 49–58.
[10] M.A. Halcrow, Spin-crossover materials properties and applications, A John Wiley & Sons Ltd, Chichester, 2013.
[11] H. Lin, D. Siretanu, D.A. Dickie, D. Subedi, J.J. Scepaniak, D. Mitcov, R. Cle, J. M. Smith, Am. Chem. Soc. 136 (2014) 13326–13332.
[12] K. Senthil, M. Ruben, Coord. Chem. Rev. 346 (2017) 176–205.

[13] J.F. Létard, P. Guionneau, O. Nguyen, J.S. Costa, S. Marcén, G. Chastanet, M. Marchivie, L. Goux-Capes, Chem. - A Eur. J. 11 (2005) 4582–4589.
[14] J.F. Létard, P. Guionneau, L. Rabardel, J.A.K. Howard, A.E. Goeta, D. Chasseau, O. Kahn, Inorg. Chem. 37 (1998) 4432–4441.
[15] P. Gütlich, A. Hauser, H. Spiering, Angew. Chemie Int. Ed. 33 (1994).
[16] P. Gutlich, S. Decurtins, K.M. Hasselbach, H. Spiering, A. Hauser, Inorg. Chem. 24 (1985) 2174–2178.
[17] O. Kahn, J. Krober, C. Jay, Adv. Mater. 4 (1992) 718–728.
[18] A.B. Gaspar, M.C. Mun, J. Mater. Chem. 16 (2006) 2522–2533.
[19] A. Hauser, Spin-Crossover Materials. Properties and Applications, John Wiley & Sons,, Hoboken, 2013.
[20] C. Rajnak, J. Titis, O. Fuhr, M. Ruben, R. Boca, Polyhedron 123 (2017) 122–131.
[21] W.J. Stratton, D.H. Busch, J. Am. Chem. Soc. 80 (1958) 1286–1289.
[22] W.K. Han, Z.H. Li, W. Zhu, T. Li, Z. Li, X. Ren, Z.G. Gu, Dalt. Trans. 46 (2017) 4218–4224.
[23] Y.T. Wang, S.T. Li, S.Q. Wu, A.L. Cui, D.Z. Shen, H.Z. Kou, J. Am. Chem. Soc. 135 (2013) 5942–5945.
[24] H. Hagiwara, T. Tanaka, S. Hora, Dalt. Trans. 45 (2016) 17132–17140.
[25] N. Struch, J.G. Brandenburg, G. Schnakenburg, N. Wagner, J. Beck, S. Grimme, A. Lützen, Eur. J. Inorg. Chem. 2015 (2015) 5503–5510.
[26] J.R. Thompson, R.J. Archer, C.S. Hawes, A. Ferguson, A. Wattiaux, C. Mathonière, R. Clérac, P.E. Kruger, Dalt. Trans. 41 (2012) 12720–12725.
[27] Y. Garcia, V. Niel, M. Carmen Muñoz, J.A. Real, Top. Curr. Chem. 233 (2004) 229–257.
[28] W. Qin, S. Long, M. Panunzio, S. Biondi, Molecules 18 (2013) 12264–12289.
[29] F. Elemo, T. Sani, M. Thomas, Transit. Met. Chem. 47 (2022) 265–274.
[30] A.B. Gaspar, B. Weber, Spin Crossover Phenomenon in Coordination Compounds: First edition, Wiley-VCH Verlag GmbH & Co. KGaA, 2017, 231–252.
[31] Y. Qiu, L. Cui, J. Ge, M. Kurmoo, G. Ma, B. Weber, Front. Chem. 9 (2021) 2–9.
[32] C. Lochenie, W. Bauer, A.P. Railliet, S. Schlamp, Y. Garcia, B. Weber, Inorg. Chem. 53 (2014) 11563–11572.
[33] K. Fujita, R. Kawamoto, R. Tsubouchi, Y. Sunatsuki, M. Kojima, S. Iijima, N. Matsumoto, Chem. Lett. 36 (2007) 1284–1285.
[34] M.A. Fik, M. Löffler, M. Weselski, M. Kubicki, M.J. Korabik, V. Patroniak, Polyhedron 102 (2015) 609–614.
[35] J.S. Miller, D. Gatteschi, Chem. Soc. Rev. 40 (2011) 3313–3335.
[36] S. Alshehri, J. Burgess, J. Fawcett, D.R. Russell, A.M. Shaker, Transit. Met. Chem. 25 (2000) 691–694.
[37] N.T. Madhu, I. Salitros, F. Schramm, S. Klyatskaya, O. Fuhr, M. Ruben, Rendus Chim. 11 (2008) 1166–1174.
[38] G.M. Sheldrick, Acta Crystallogr. Sect. A. Crystallogr. 71 (2015) 3–8.
[39] G.M. Sheldrick, Acta Crystallogr. Sect. C, Struct. Chem. 71 (2015) 3–8.
[40] A. Garza-Ortiz, P.U. Maheswari, M. Siegler, A.L. Spek, J. Reedijk, Inorg. Chem. 47 (2008) 6964–6973.
[41] T. TURBOMOLE, version 7.5, TURBOMOLE GmBH, a development of the University of Karlsruhe and Forschungszentrum Karlsruhe, 2020; available from: http://www.turbomole.com.
[42] J. Tao, J.P. Perdew, V.N. Staroverov, G.E. Scuseria, Phys. Rev. Lett. 91 (2003) 3–6.
[43] S. Grimme, J. Antony, S. Ehrlich, H. Krieg, J. Chem. Phys. 132 (2010).
[44] S. Grimme, S. Ehrlich, L. Goerigk, J. Comput. Chem. 32 (2011) 1456–1465.
[45] F. Weigend, R. Ahlrichs, Phys. Chem. Chem. Phys. 7 (2005) 3297–3305.
[46] Gaussian 16, Revision C.01, Frisch, M. J.; Trucks, G. W.; Schlegel, H. B.; Scuseria, G. E.; Robb, M. A.; Cheeseman, J. R.; Scalmani, G.; Barone, V.; Petersson, G. A.; Nakatsuji, H.; Li, X.; Caricato, M.; Marenich, A. V.; Bloino, J.; Janesko, B. G.; Gomper, III (2016) 2016.
[47] J. Tomasi, B. Mennucci, R. Cammi, Chem. Rev. 105 (2005) 2999–3093.
[48] K. Nakamoto, Infrared and Raman Spectra of Inorganic and Coordination Compounds: Part A: Theory and Applications in Inorganic Chemistry, Sixth Edition, 2008.
[49] S. Hora, H. Hagiwara, Inorganics. 5 (2017) 49.
[50] A.D.Buckingham and P.J. Stephen, *Chem. Soc*., (1964) 4583–4587.
[51] A.D.Buckingham and P.J. Stephen, *Chem. Soc*., (1964) 2747–2759.
[52] P. Hrobarik, F. Peter, M. Meier, S. Repisk, M.K. Komorovsk, J. Phys. Chem. A. 115 (2011) 5654–5659.
[53] J.E. Barquera-lozada, A. Obenhuber, C. Hauf, W. Scherer, J. Phys. Chem. A. 117 (2013) 4304–4315.
[54] Y. Ruiz-morales, G. Schreckenbach, T. Ziegler, Organometallics 15 (1996) 3920–3923.
[55] J.K. Beattie, Adv. Inorg. Chem. 32 (1988) 1–53.
[56] Y. Sunatsuki, R. Kawamoto, K. Fujita, H. Maruyama, T. Suzuki, H. Ishida, M. Kojima, S. Iijima, N. Matsumoto, Inorg. Chem. 48 (2009) 8784–8795.
[57] S. Ghosh, S. Kamilya, T. Pramanik, M. Rouzières, R. Herchel, S. Mehta, A. Mondal, Inorg. Chem. 59 (2020) 13009–13013.
[58] S. Ghosh, S. Kamilya, T. Pramanik, A. Mohanty, M. Rouzières, R. Herchel, S. Mehta, A. Mondal, Dalt. Trans. 50 (2021) 7725–7735.
[59] G.S. Matouzenko, G. Molnar, N. Bréfuel, M. Perrin, A. Bousseksou, S.A. Borshch, Chem. Mater. 15 (2003) 550–556.
[60] K. Sugimoto, T. Okubo, M. Maekawa, T. Kuroda-Sowa, *Cryst. Growth Des*. 21 (2021) 4178–4183.
[61] M. Buron-Le Cointe, J. Hébert, C. Baldé, N. Moisan, L. Toupet, P. Guionneau, J. F. Létard, E. Freysz, H. Cailleau, E. Collet, Phys. Rev. B - Condens. Matter Mater. Phys. 85 (2012) 39–41.
[62] K. Senthil Kumar, S. Vela, B. Heinrich, N. Suryadevara, L. Karmazin, C. Bailly, M. Ruben, *Dalt. Trans.* 49 (2020) 1022–1031.

**Electronic Supplementary Information**

# Spin state of two mononuclear iron(II) complexes of a tridentate pyridine-diimine N-donor ligand: Experimental and theoretical investigations

**Yosef Bayeh[a,b,c], Patrik Osuský[b], Nathan J. Yutronkie[d], Róbert Gyepes[e], Assefa Sergawie[a], Peter Hrobárik[b], Rodolphe Clérac[d] and Madhu Thomas[a,c*]**

[a] Department of Industrial Chemistry, College of Applied Sciences, Addis Ababa Science and Technology University, P.O. Box 16417, Addis Ababa, Ethiopia

[b] Department of Inorganic Chemistry, Faculty of Natural Sciences, Comenius University, Mlynská dolina CH-2, Ilkovičova 6, 84215 Bratislava, Slovakia

[c] Nanotechnology Centre of Excellence, Addis Ababa Science and Technology University, Addis Ababa P.O. Box 16417, Ethiopia

[d] Univ. Bordeaux, CNRS, Centre de Recherche Paul Pascal, CRPP, UMR 5031, 33600 Pessac, France

[e] Department of Inorganic Chemistry, Faculty of Science, Charles University in Prague, Hlavova 2030/8, 12843 Prague, Czech Republic

madhu.thomas@aastu.edu.et

**Content (25 pages)**

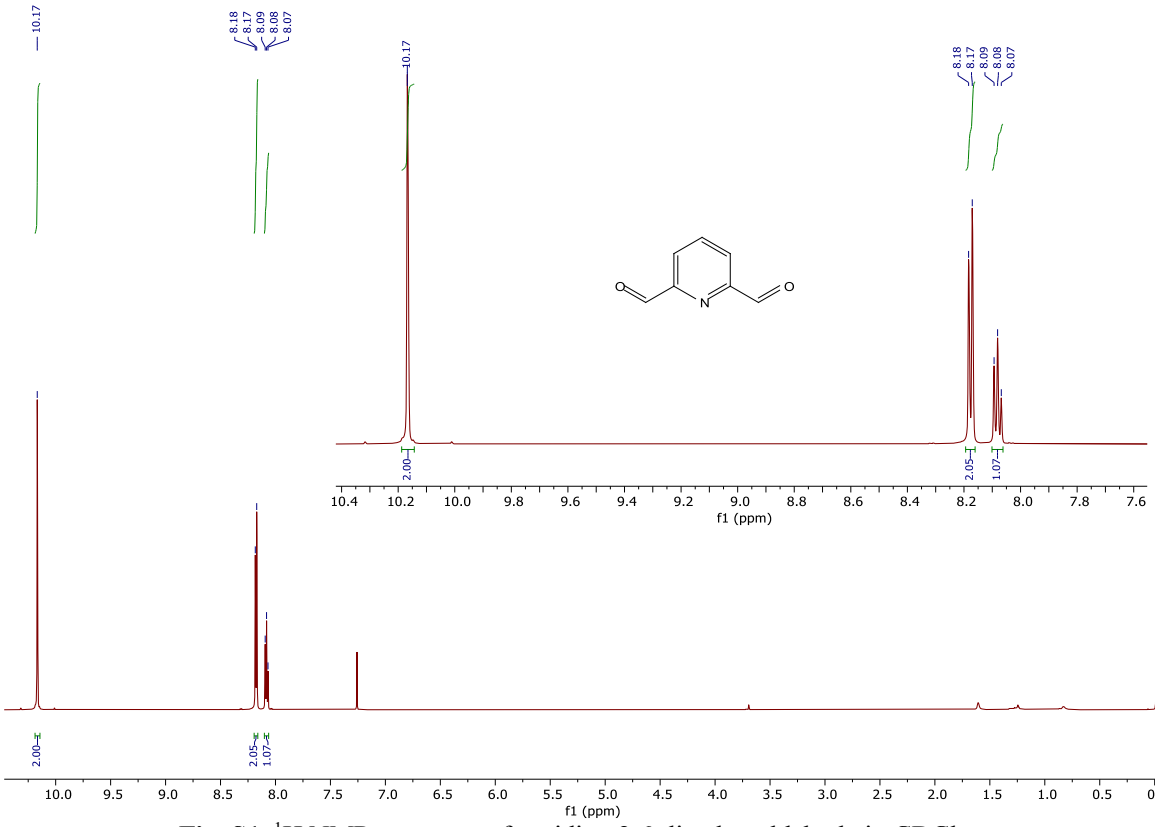


**Fig. S1.** $^{1}$H NMR spectrum of pyridine-2,6-dicarboxaldehyde in $CDCl_3$

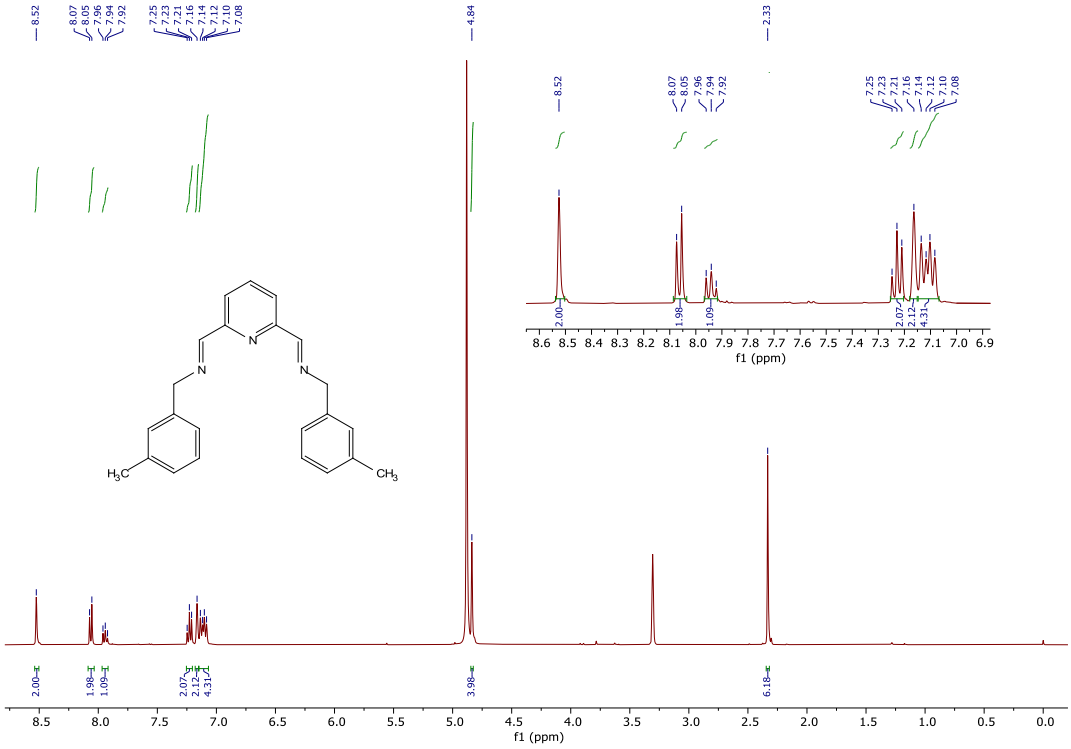


**Fig. S2.** $^{1}$H NMR spectrum of **L** in $CH_3OH$-$d_4$

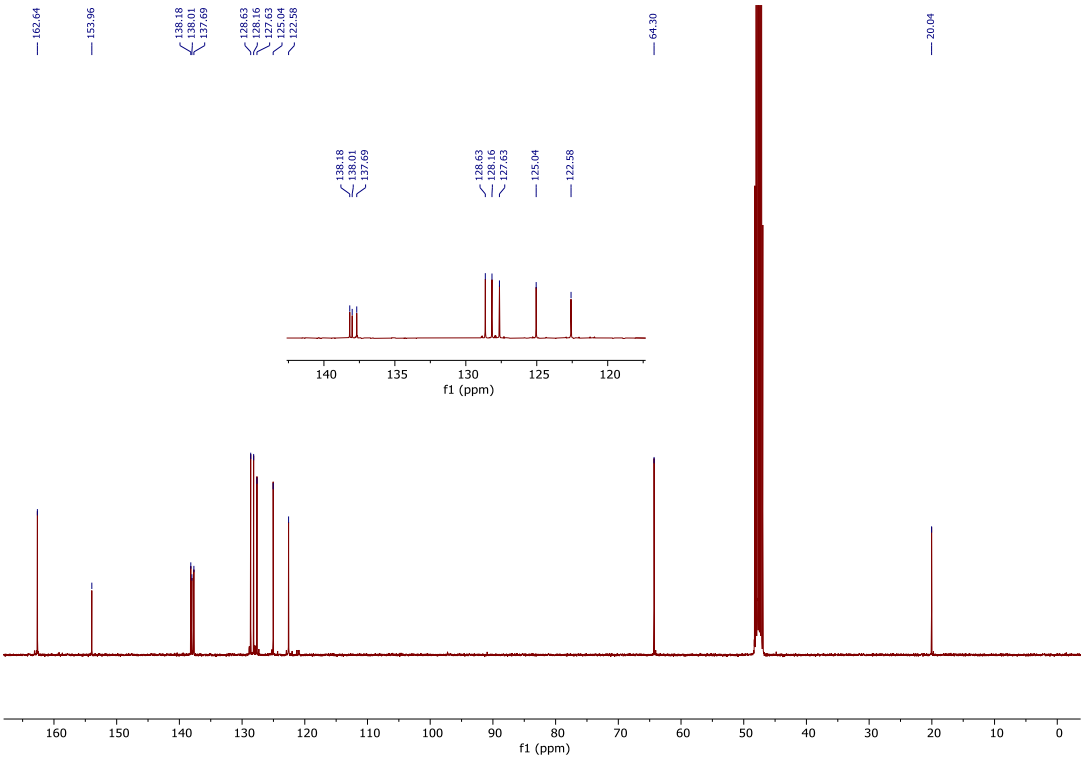


**Fig. S3.** $^{13}$C NMR spectrum of **L** in $CH_3OH$-$d_4$

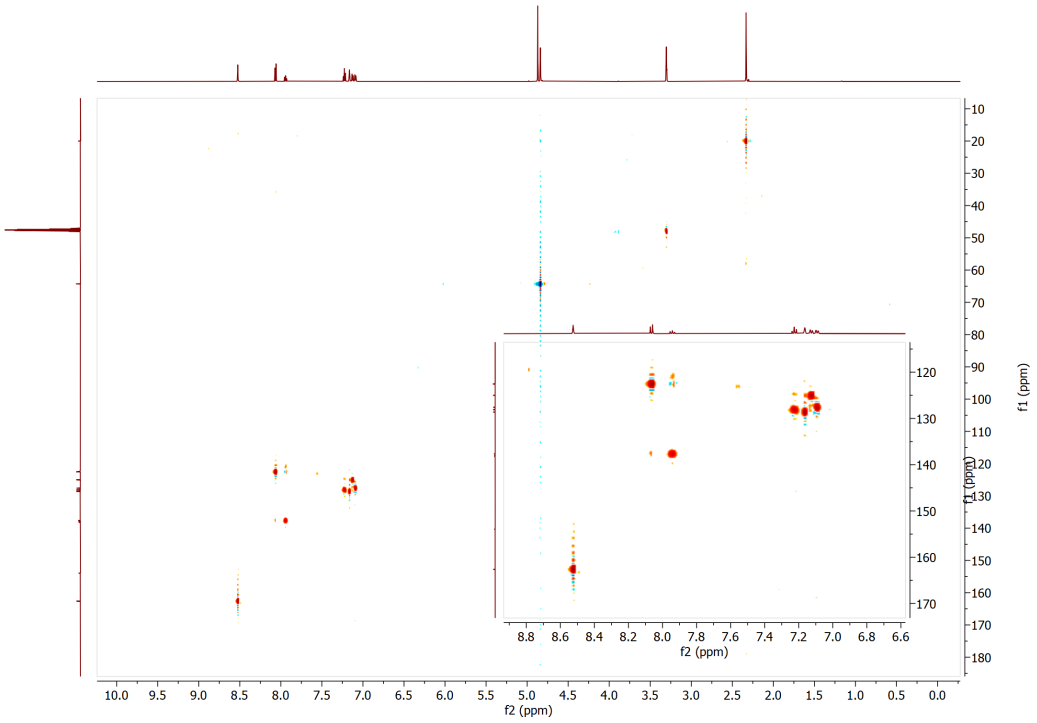


(a)

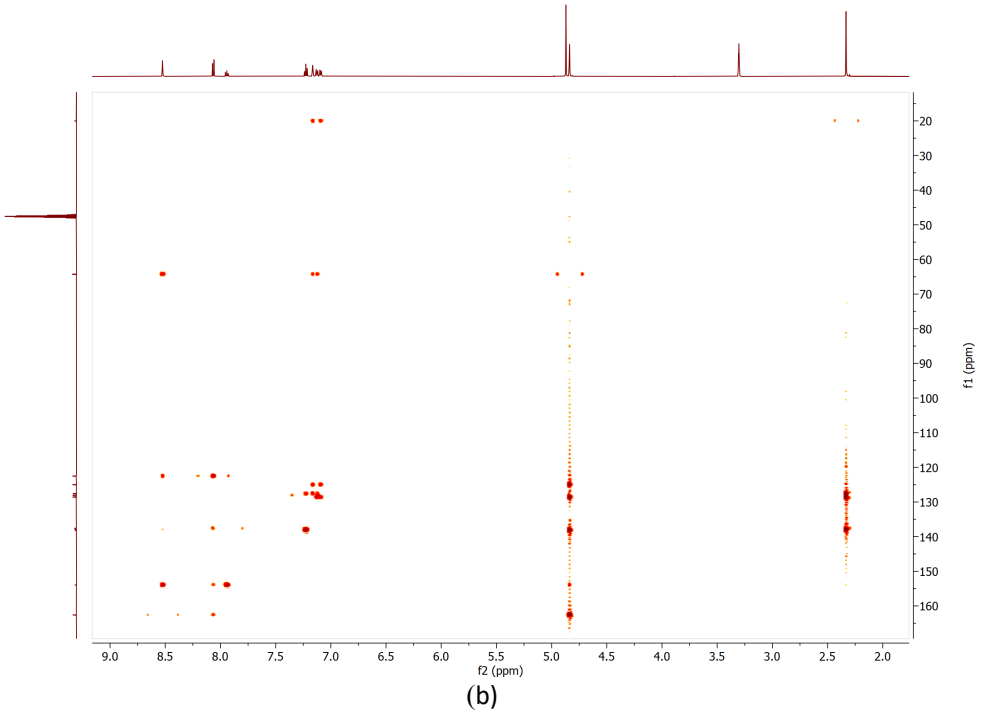


(b)

**Fig. S4.** (a) $^{1}$H-$^{13}$C HSQC and (b) $^{1}$H-$^{13}$C HMBC NMR spectra of **L** in $CH_3OH$-$d_4$

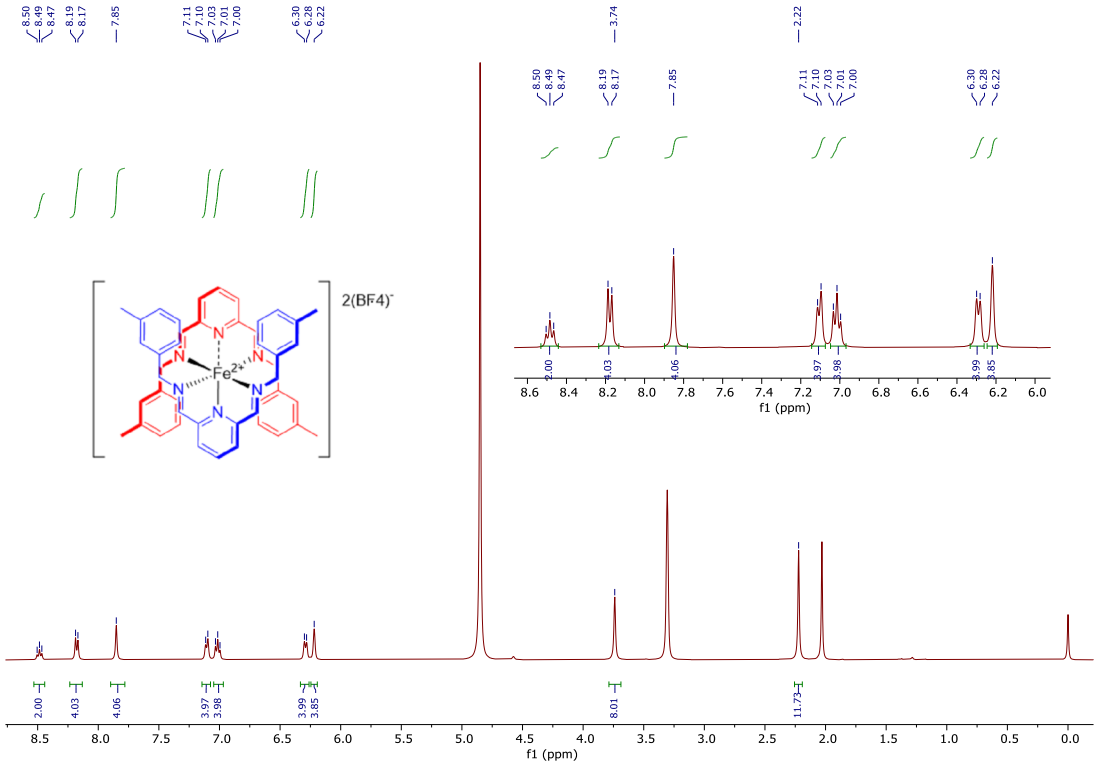


**Fig. S5.** $^{1}$H NMR spectrum of **2** in $CH_3OH$-$d_4$

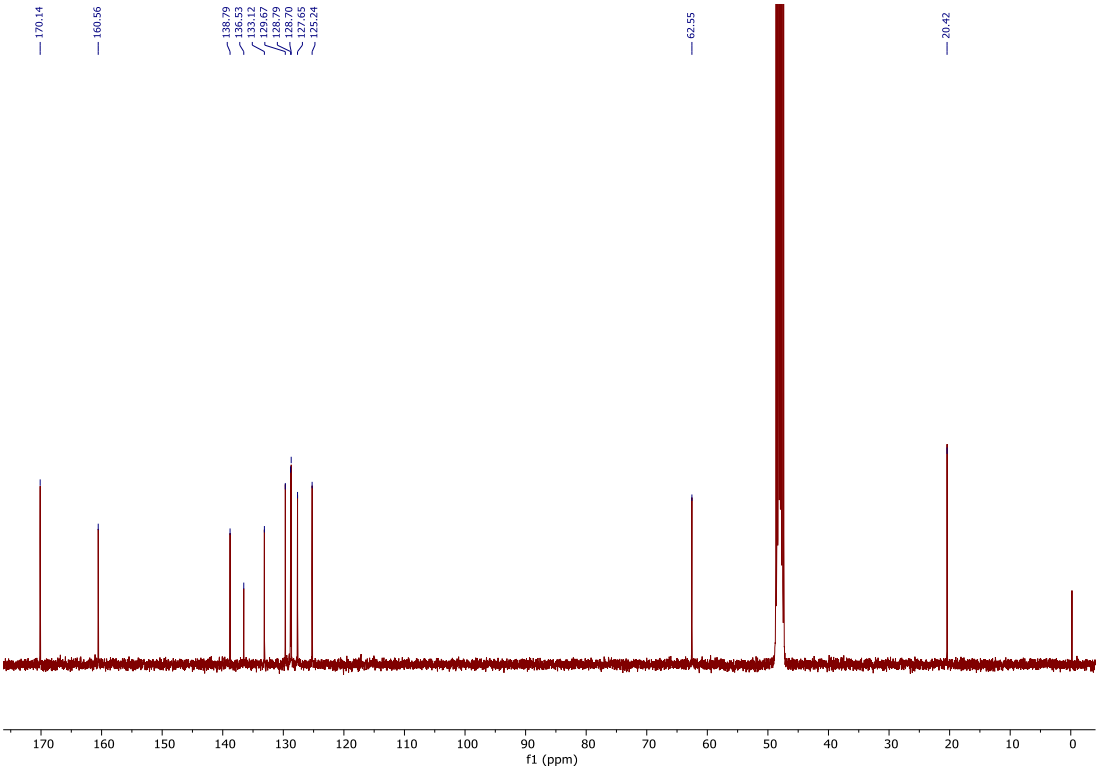


**Fig. S6.** $^{13}$C NMR spectrum of **2** in $CH_3OH$-$d_4$

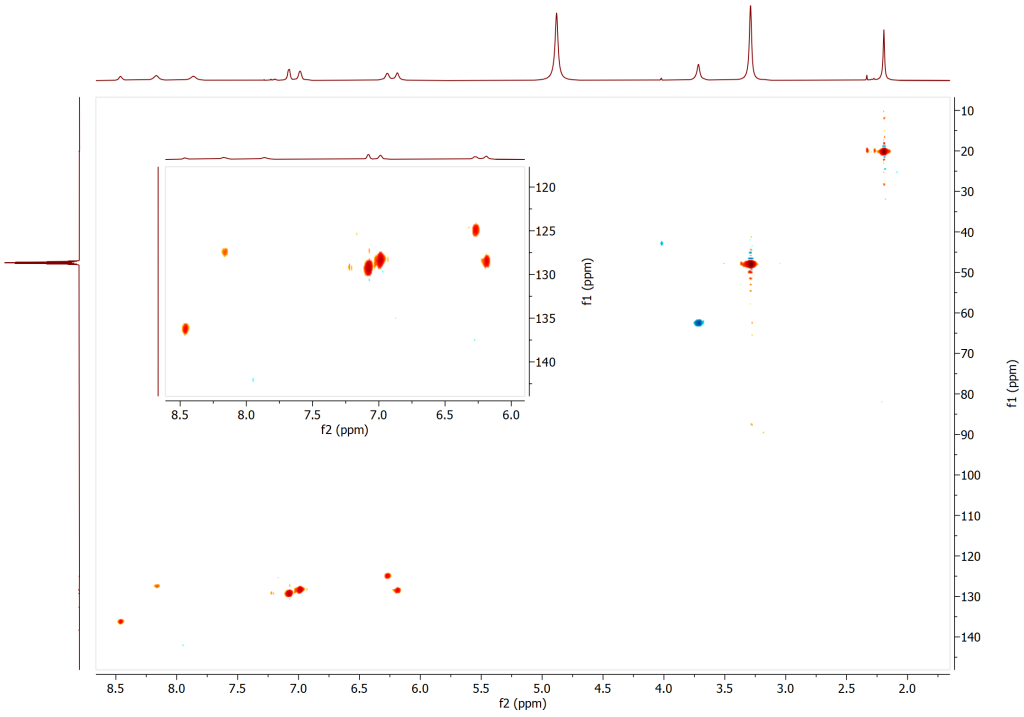


(a)

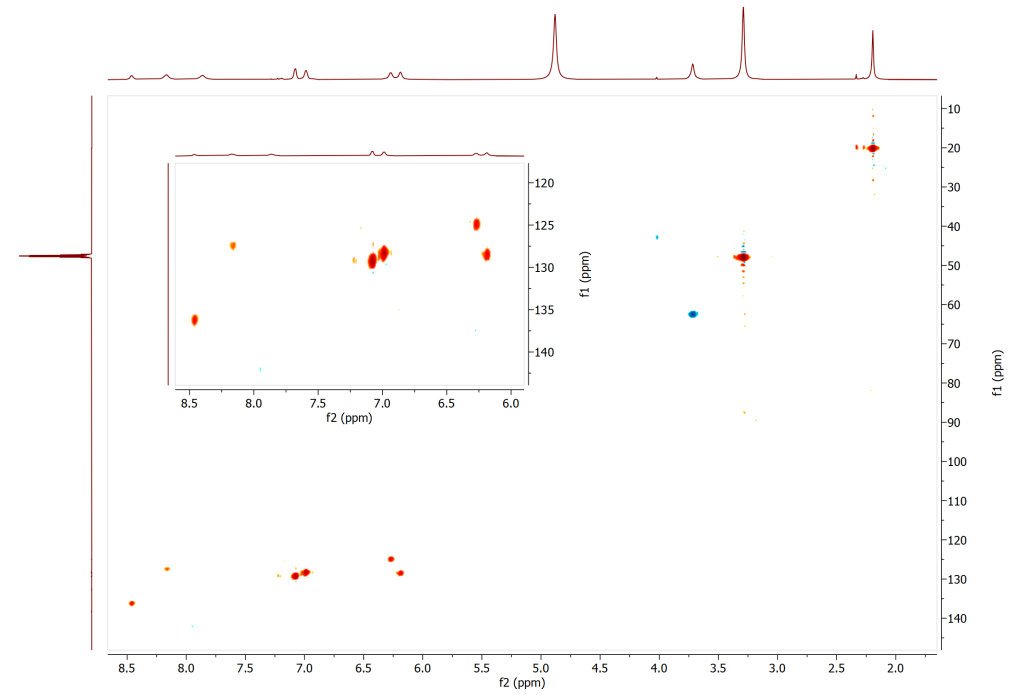


(b)

**Fig. S7.** (a) $^{1}$H-$^{13}$C HSQC and (b) $^{1}$H-$^{13}$C HMBC NMR spectra of **2** in $CH_3OH$-$d_4$

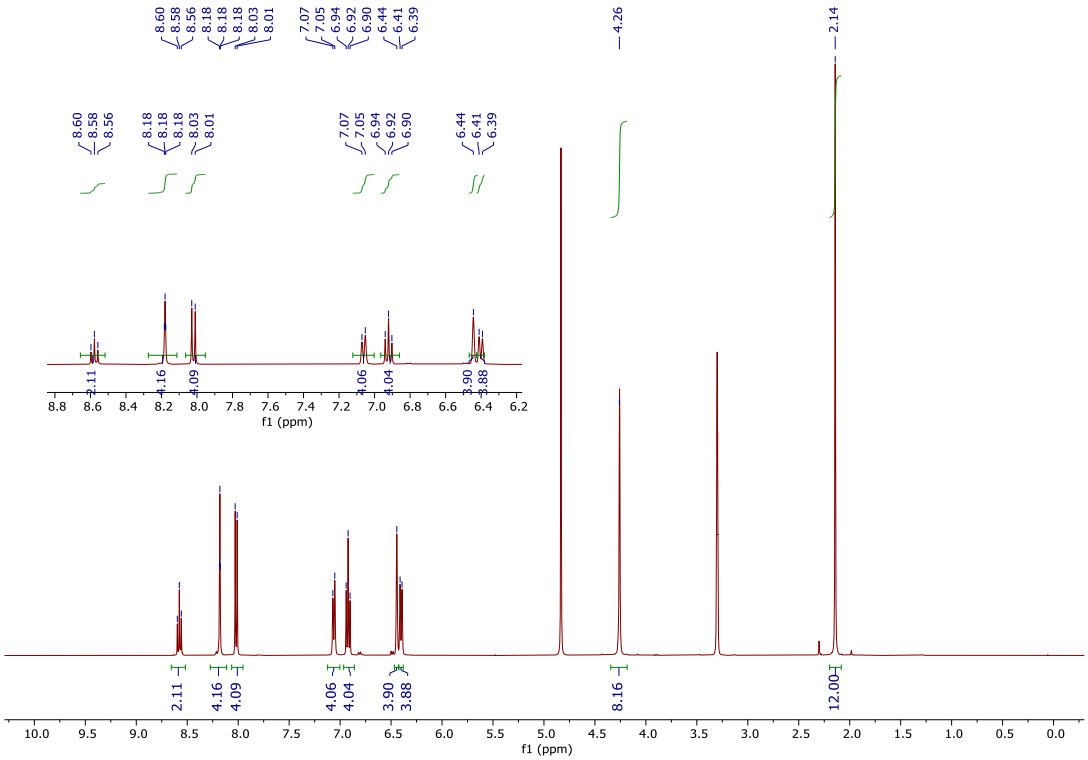


**Fig. S8.** $^{1}$H NMR spectrum of **3** in $CH_3OH$-$d_4$

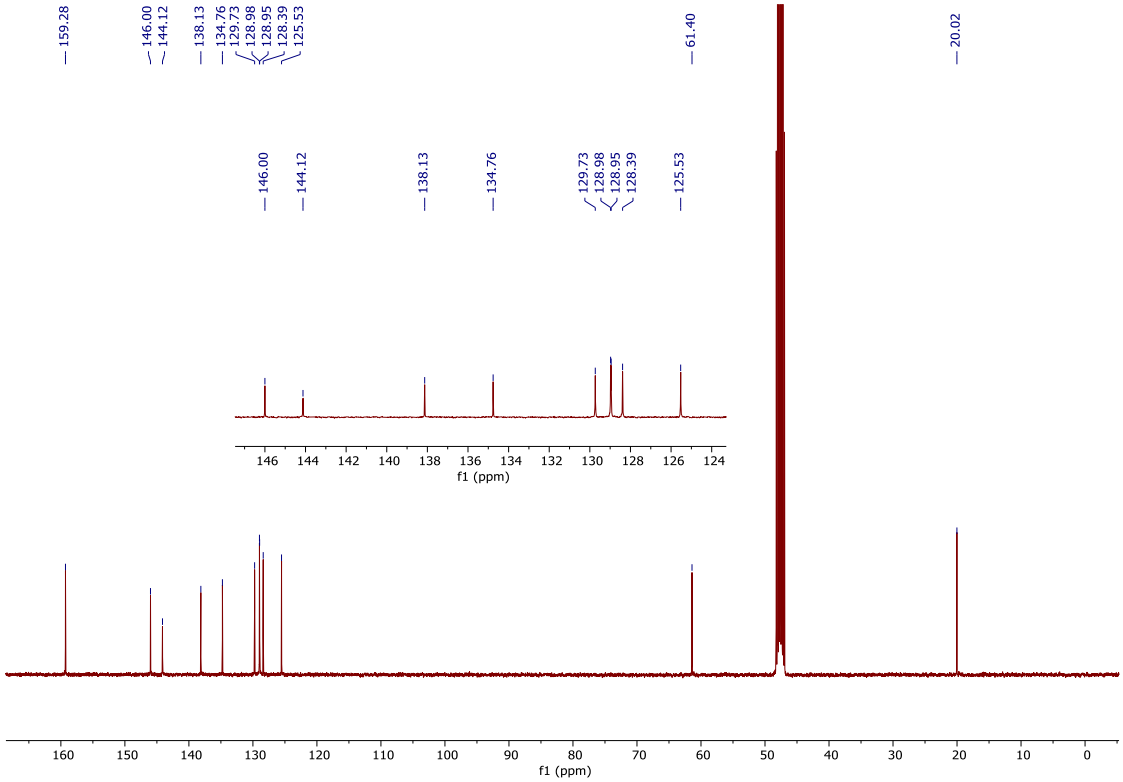


**Fig. S9.** $^{13}$C NMR spectrum of **3** in $CH_3OH$-$d_4$

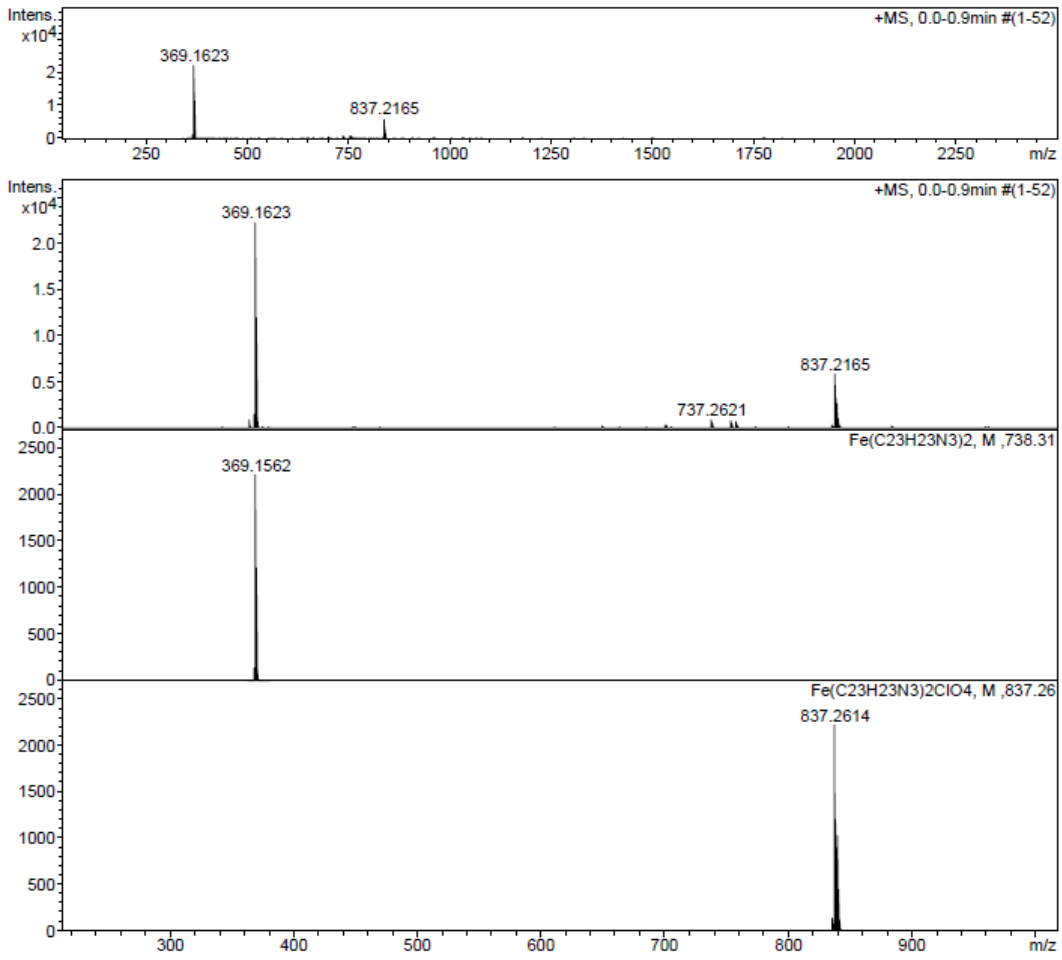
Intens.
x10^4
+MS, 0.0-0.9min #(1-52)
369.1623
837.2165
m/z
737.2621
Fe(C23H23N3)2, M ,738.31
369.1562
Fe(C23H23N3)2ClO4, M ,837.26
837.2614

(a)

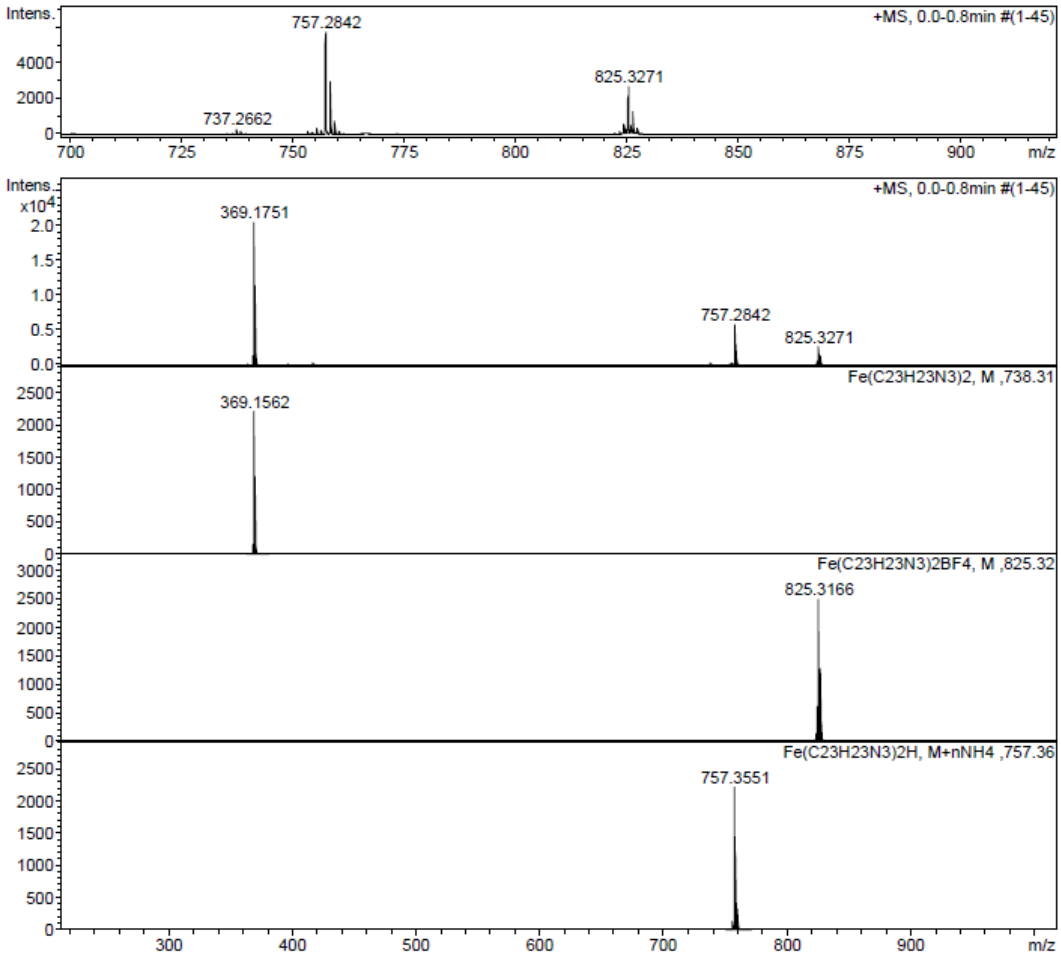


(b)

**Fig. S10**. ESI-MS molecular ion peaks of **1** (a) and **2** (b).

**Table S1**. Selected bond lengths [Å] for **L**.

| Parameter | **L** |
|---|---|
| N(1)-C(5) | 1.3434(12) |
| N(1)-C(1) | 1.3466(12) |
| N(2)-C(7) | 1.4587(12) |
| N(3)-C(16) | 1.4604(12) |
| Av. N-C | 1.4075 |

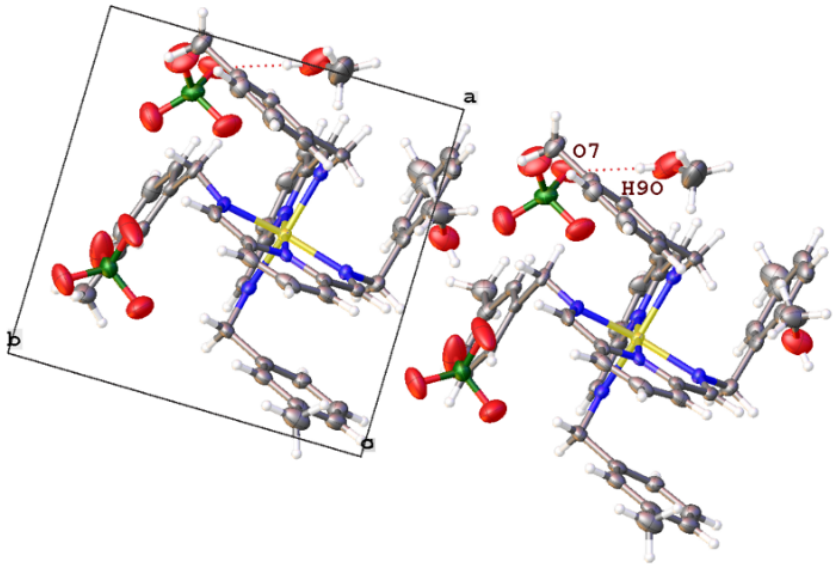


(a)

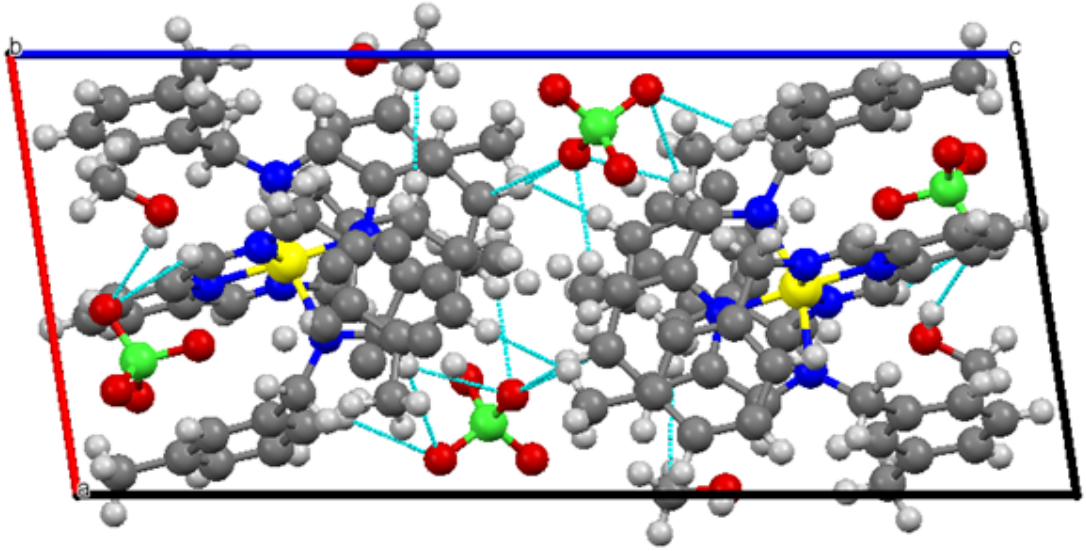


(b)

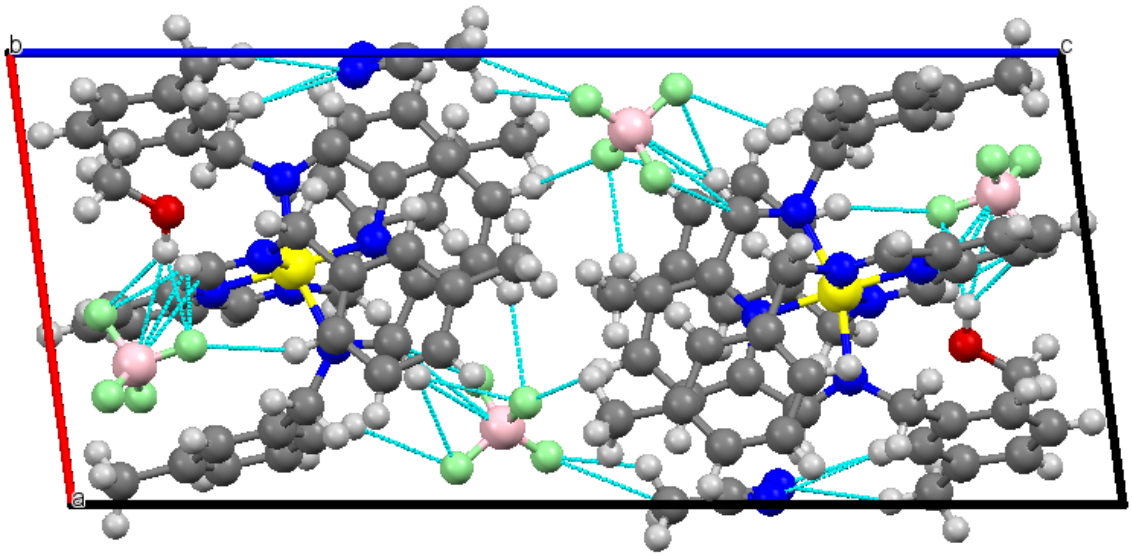


(c)

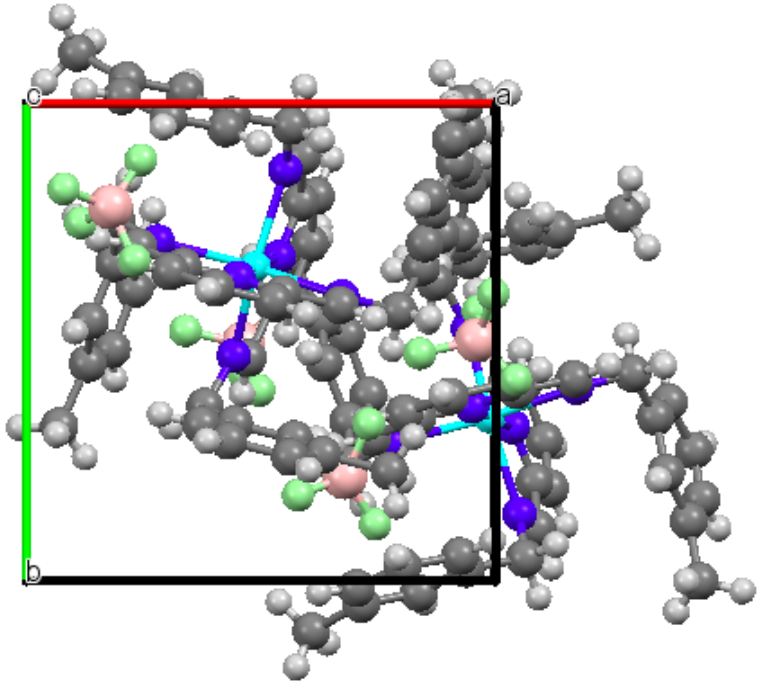


(d)

**Fig. S11.** Projection of the π-π interaction through phenyl rings of **1** (a) along the *bc*-plane. Crystallographic views illustrating the short intermolecular contacts and H-bonding and crystal packing in **1** (b) and **2** (c) down the *b*-direction. Crystal packing of **3** (d). Color codes: Yellow Fe, blue N, black C, grey H, green Cl, red O, pink B and light green F.

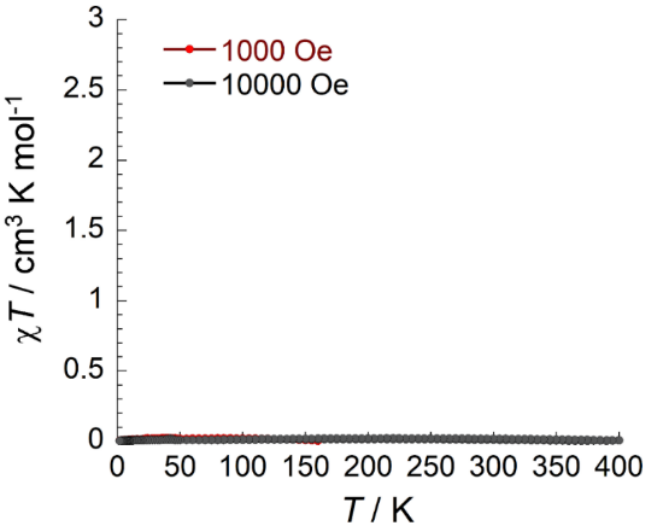


(a)

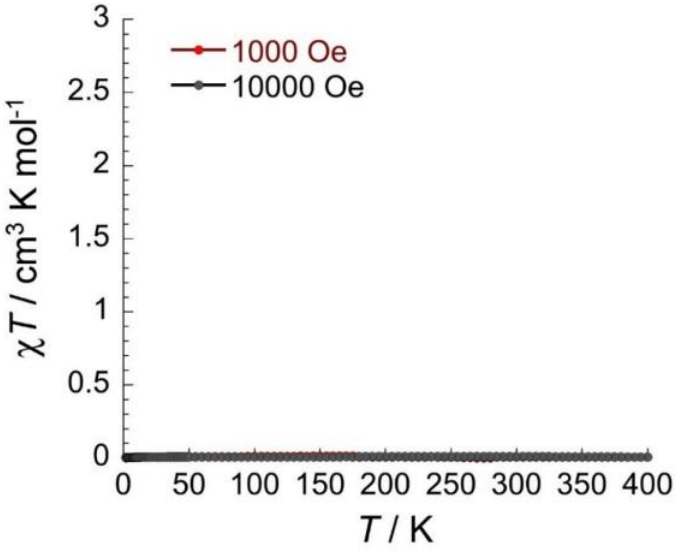


(b)

**Fig. S12.** Temperature dependence of the $\chi T$ product for (a) **1** and (b) **2** discussed in this paper at 0.1 and 1 T ($\chi$ is defined as $M/H$ per mole of the respective complex).

**Table S2.** Experimental and computed $^{1}$H NMR shifts (in ppm vs. TMS) in the free ligand **L** and corresponding $[Fe(\mathbf{L})_2]^{2+}$ and $[Zn(\mathbf{L})_2]^{2+}$ complexes (all in $CH_3OH$-$d_4$) [a]

| | H-imine | py-3,5 | py-4 | $CH_2$ | H-2 | H-4 | H-5 | H-6 | $CH_3$ |
|---|---|---|---|---|---|---|---|---|---|
| **L** | | | | | | | | | |
| **Expt.** | 8.52 | 8.06 | 7.94 | 4.84 | 7.16 | 7.09 | 7.23 | 7.12 | 2.33 |
| **Calcd.** | 8.39 | 8.21 | 7.64 | 4.66 | 6.98 | 6.91 | 6.97 | 6.49 | 2.04 |
| **$[Fe(L)_2]^{2+}$** | | | | | | | | | |
| **Expt.** | 7.85 | 8.18 | 8.49 | 3.74 | 6.22 | 7.11 | 7.01 | 6.29 | 2.22 |
| **Calcd.** | 7.53 | 7.63 | 8.16 | 3.71 | 5.98 | 6.84 | 7.01 | 6.11 | 2.04 |
| **$[Zn(L)_2]^{2+}$** | | | | | | | | | |
| **Expt.** | 8.18 | 8.03 | 8.58 | 4.26 | 6.44 | 7.06 | 6.92 | 6.40 | 2.14 |
| **Calcd.** | 7.66 | 7.69 | 8.38 | 3.72 | 5.86 | 6.8 | 6.99 | 6.32 | 1.94 |

[a] Calculations done at the TPSSh-D3(BJ)/def2-TZVP/PCM($CH_3OH$) level.

**Table S3.** Experimental and computed $^{13}C$ NMR shifts (in ppm vs. TMS) in the free ligands **L** and corresponding $[Fe(\mathbf{L})_2]^{2+}$ and $[Zn(\mathbf{L})_2]^{2+}$ complexes (all in $CH_3OH$-$d_4$) [a]

| | C-imine | py-2,6 | py-3,5 | py-4 | $CH_2$ | C-1 | C-2 | C-3 | C-4 | C-5 | C-6 | $CH_3$ |
|---|---|---|---|---|---|---|---|---|---|---|---|---|
| **L** | | | | | | | | | | | | |
| **Expt.** | 162.6 | 154.0 | 122.6 | 137.7 | 64.3 | 138.2 | 128.6 | 138.1 | 127.6 | 128.2 | 125.0 | 20.0 |
| **Calcd.** | 164.7 | 152.9 | 120.1 | 133.9 | 65.1 | 139.8 | 124.7 | 137.4 | 123.8 | 124.5 | 119.5 | 19.5 |
| **$[Fe(L)_2]^{2+}$** | | | | | | | | | | | | |
| **Expt.** | 170.1 | 160.6 | 127.7 | 136.5 | 62.6 | 133.1 | 128.8 | 138.8 | 129.7 | 128.7 | 125.2 | 20.4 |
| **Calcd.** | 166.6 | 156.2 | 125.9 | 133.5 | 63.7 | 131.2 | 126.4 | 139.4 | 127.6 | 125.4 | 122.1 | 19.1 |
| **$[Zn(L)_2]^{2+}$** | | | | | | | | | | | | |
| **Expt.** | 159.3 | 144.1 | 129.7 | 146.0 | 61.4 | 134.8 | 129.0 | 138.1 | 129.0 | 128.4 | 125.5 | 20.0 |
| **Calcd.** | 153.8 | 144.7 | 127.8 | 141.6 | 62.1 | 133.6 | 127.3 | 138.5 | 127.4 | 125.8 | 124.0 | 19.4 |

[a] Calculations done at the TPSSh-D3(BJ)/def2-TZVP/PCM ($CH_3OH$) level.

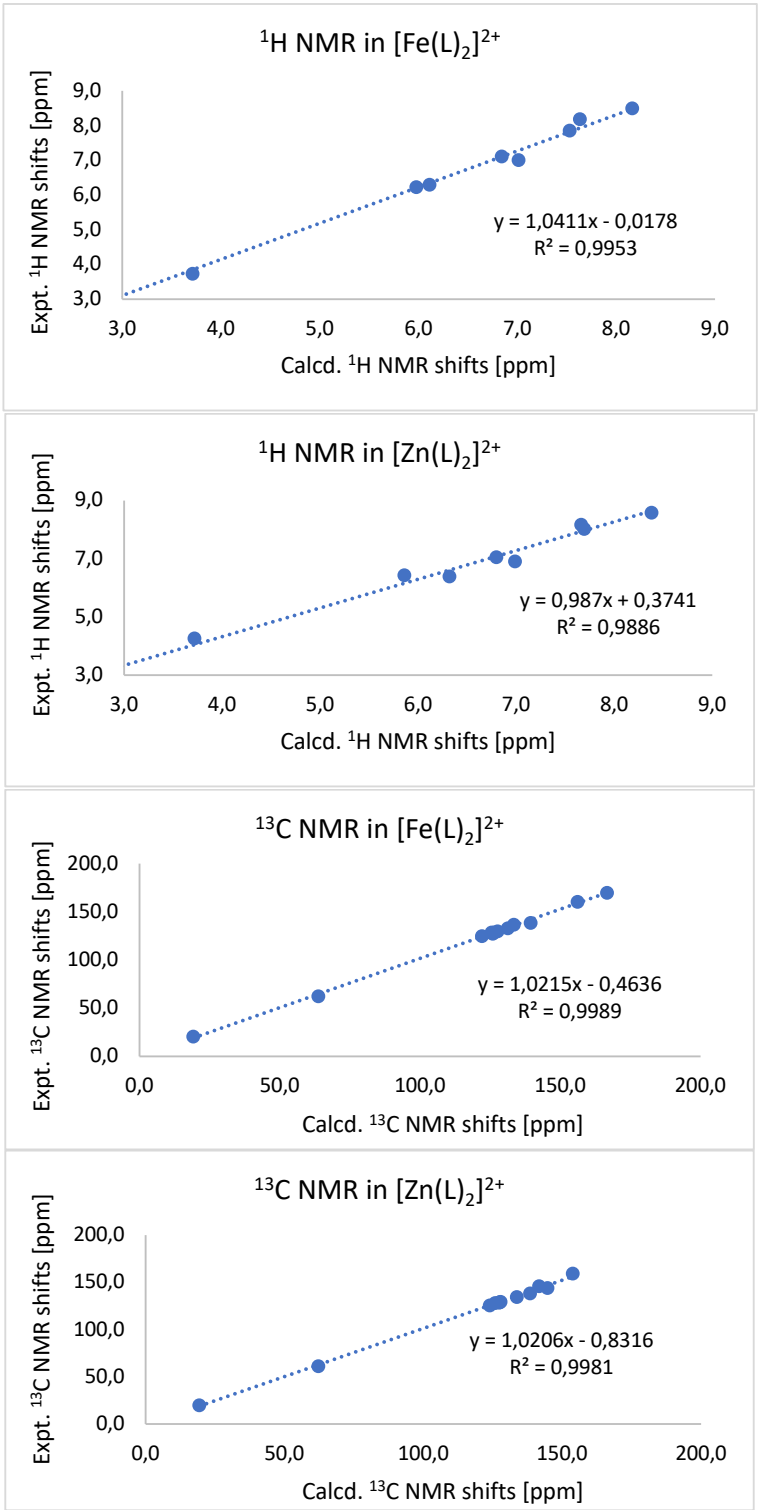


**Fig. S13.** Comparison of calculated and experimental NMR shifts in $[FeL_2]^{2+}$ and $[ZnL_2]^{2+}$ ($S$ = 0) complexes (cf. Tables S1 and S2 for numeric data)

**Table S4.** Effect of replacing the central metal-ion (Zn(II)→Fe(II)) on selected computed $^{13}$C NMR shifts (in ppm vs. TMS) considering different geometries [a]

| **System** | geometry | M | *d*(M-$N_{py}$) | *d*(M-$N_{imine}$) | Calcd. $^{13}$C NMR shifts [ppm] | | | | | |
|---|---|---|---|---|---|---|---|---|---|---|
| | | | [Å] | [Å] | **C-imine** | **py-2,6** | **py-3,5** | **py-4** | **$CH_2$** | **C-1** |
| **$[Zn(L)_2]^{2+}$** | $[Zn(L)_2]^{2+}$ | Zn | 2.083 | 2.240 | 153.8 | 144.7 | 127.8 | 141.6 | 62.1 | 133.6 |
| **$[Zn(L)_2]^{2+}$** | $[Fe(L)_2]^{2+}$ | Zn | 1.881 | 1.983 | 161.8 | 144.9 | 127.5 | 140.7 | 61.9 | 132.0 |
| **$[Fe(L)_2]^{2+}$** | $[Zn(L)_2]^{2+}$ | Fe | 2.083 | 2.240 | 158.1 | 158.3 | 127.5 | 138.0 | 64.5 | 133.4 |
| **$[Fe(L)_2]^{2+}$** | $[Fe(L)_2]^{2+}$ | Fe | 1.881 | 1.983 | 166.6 | 156.2 | 125.9 | 133.5 | 63.7 | 131.2 |

[a] Calculations done at the TPSSh-D3(BJ)/def2-TZVP/PCM ($CH_3OH$) level.

DFT optimized Cartesian coordinates of the ligand **L**, its Fe(II) complexes $[Fe(\mathbf{L})_2]^{2+}$ in S=0 and S=2 spin-states and Zn(II) congener $[Zn(\mathbf{L})_2]^{2+}$

TPSSh-D3(BJ)/def2-TZVP results *in vacuo*

**L**

49

Energy=-1055.054409774

| | | | |
|---|---|---|---|
| N | -0.50316 | -0.31198 | -1.25142 |
| N | 2.74817 | 0.08223 | -2.62983 |
| N | -3.80416 | 0.07876 | 0.00451 |
| C | -1.62542 | 0.36028 | -0.96304 |
| C | 5.12613 | -0.32053 | -2.13579 |
| C | 3.88365 | -0.78560 | -2.86648 |
| H | 4.08838 | -0.77235 | -3.94242 |
| H | 3.66316 | -1.82865 | -2.58690 |
| C | 0.50508 | 0.36067 | -1.82204 |
| C | 6.37616 | -0.78017 | -2.55376 |
| H | 6.43826 | -1.43619 | -3.41828 |
| C | 5.05093 | 0.52449 | -1.03309 |
| H | 4.08753 | 0.89631 | -0.70745 |
| C | -2.69279 | -0.43425 | -0.33226 |
| H | -2.44594 | -1.49304 | -0.17735 |
| C | -6.39269 | -0.72931 | 2.55261 |
| H | -7.06423 | -1.33739 | 1.95225 |
| C | 1.71231 | -0.43295 | -2.10711 |
| H | 1.64133 | -1.49262 | -1.82776 |
| C | -6.77595 | -0.37025 | 3.84218 |
| C | 0.43265 | 1.72211 | -2.12754 |
| H | 1.28565 | 2.20174 | -2.58996 |
| C | -5.17056 | -0.32676 | 2.01055 |
| C | -1.78534 | 1.72187 | -1.23249 |
| H | -2.72046 | 2.20133 | -0.97316 |
| C | -4.31904 | 0.46260 | 2.77683 |
| H | -3.37513 | 0.79343 | 2.36201 |
| C | 7.54741 | -0.42145 | -1.89149 |
| C | -4.78547 | -0.79063 | 0.62141 |
| H | -4.43133 | -1.83339 | 0.66787 |
| H | -5.68025 | -0.77678 | -0.00971 |
| C | -4.69045 | 0.83516 | 4.06622 |
| H | -4.02599 | 1.45381 | 4.65899 |
| C | 6.21314 | 0.89404 | -0.36152 |
| H | 6.15074 | 1.55201 | 0.49803 |
| C | -0.73496 | 2.40781 | -1.82513 |
| H | -0.82540 | 3.46441 | -2.04904 |
| C | -5.90464 | 0.42167 | 4.59631 |
| H | -6.18492 | 0.71819 | 5.60184 |
| C | 7.44949 | 0.42428 | -0.78285 |
| H | 8.34909 | 0.71545 | -0.25027 |
| C | -8.09732 | -0.81632 | 4.41098 |
| H | -8.71227 | 0.04128 | 4.69843 |
| H | -7.95348 | -1.42736 | 5.30670 |
| H | -8.65895 | -1.40733 | 3.68577 |
| C | 8.88850 | -0.91039 | -2.37183 |
| H | 9.42555 | -0.11846 | -2.90343 |
| H | 8.77959 | -1.75487 | -3.05466 |
| H | 9.51740 | -1.22492 | -1.53545 |

$[Fe(\mathbf{L})_2]^{2+}$ (S=0)

99

Energy=-3373.642851606

| | | | |
|---|---|---|---|
| Fe | 5.59934 | 6.52974 | 5.66687 |
| N | 7.46421 | 6.06638 | 6.15400 |
| N | 5.84762 | 6.81107 | 3.82330 |
| N | 5.24616 | 4.70241 | 4.97931 |
| N | 5.39765 | 6.24603 | 7.51479 |
| N | 3.65732 | 6.87920 | 5.87179 |
| N | 5.99468 | 8.47527 | 5.65727 |
| C | 6.12468 | 8.05166 | 3.37569 |
| C | 6.48396 | 5.95865 | 8.25858 |
| C | 5.71684 | 3.07558 | 6.78941 |
| C | 4.73927 | 3.56310 | 5.75007 |
| H | 4.46494 | 2.76087 | 5.05820 |
| H | 3.82408 | 3.90020 | 6.24119 |
| C | 5.77193 | 5.76444 | 2.98026 |
| C | 9.25121 | 6.87794 | 3.07698 |
| H | 9.10028 | 5.91322 | 2.60184 |
| C | 8.57512 | 5.80393 | 5.23362 |

| | | | | | | | |
|---|---|---|---|---|---|---|---|
| H | 8.23092 | 5.02850 | 4.54484 | H | 9.81555 | 10.28680 | 4.77834 |
| H | 9.41385 | 5.38816 | 5.80180 | C | 2.73513 | 7.31838 | 4.81945 |
| C | 4.17479 | 6.33757 | 8.06991 | H | 3.20638 | 8.15627 | 4.30381 |
| C | 9.00786 | 7.01151 | 4.44228 | H | 1.81248 | 7.68120 | 5.28217 |
| C | 5.28272 | 2.86843 | 8.09691 | C | 6.33067 | 8.28940 | 2.02135 |
| H | 4.24854 | 3.07862 | 8.35271 | H | 6.55270 | 9.28813 | 1.67011 |
| C | 7.65435 | 5.84946 | 7.41277 | C | 7.47262 | 2.13742 | 8.73442 |
| H | 8.62057 | 5.54643 | 7.80517 | H | 8.16270 | 1.76837 | 9.48513 |
| C | 5.39227 | 4.56696 | 3.70365 | C | 7.91395 | 2.32491 | 7.42833 |
| H | 5.18542 | 3.62865 | 3.19668 | H | 8.94057 | 2.09472 | 7.16868 |
| C | 1.95983 | 4.98042 | 4.29099 | C | 2.68344 | 6.38951 | 2.47998 |
| H | 1.75476 | 4.84227 | 5.34868 | H | 3.05039 | 7.34350 | 2.11685 |
| C | 9.22063 | 8.24221 | 5.05874 | C | 9.98619 | 7.78347 | 0.84011 |
| H | 9.05869 | 8.35504 | 6.12495 | H | 9.54118 | 6.86805 | 0.44735 |
| C | 2.45782 | 6.20330 | 3.83917 | H | 11.06503 | 7.72448 | 0.67138 |
| C | 3.20092 | 6.72621 | 7.06909 | H | 9.61713 | 8.63107 | 0.25859 |
| H | 2.16320 | 6.92563 | 7.32075 | C | 1.96588 | 4.12716 | 2.05374 |
| C | 6.37223 | 5.75078 | 9.62918 | H | 1.77273 | 3.32387 | 1.35135 |
| H | 7.24875 | 5.51752 | 10.21892 | C | 4.65471 | 9.38569 | 8.85672 |
| C | 9.69146 | 7.95295 | 2.30471 | H | 5.50555 | 9.02906 | 9.43016 |
| C | 6.20471 | 8.97749 | 4.48704 | C | 4.79932 | 9.60874 | 7.49065 |
| H | 6.46279 | 10.02308 | 4.34614 | C | 2.43290 | 5.34963 | 1.58881 |
| C | 6.26281 | 7.21264 | 1.13872 | H | 2.59568 | 5.49630 | 0.52752 |
| H | 6.42616 | 7.37128 | 0.08072 | C | 3.44127 | 9.61218 | 9.50855 |
| C | 6.14342 | 2.39046 | 9.08556 | C | 2.35832 | 10.05868 | 8.74638 |
| C | 7.03735 | 2.78580 | 6.45263 | H | 1.40418 | 10.23894 | 9.22907 |
| H | 7.38169 | 2.91260 | 5.43234 | C | 1.14949 | 2.62063 | 3.91097 |
| C | 5.98746 | 5.93461 | 1.61562 | H | 1.67239 | 1.76951 | 3.46930 |
| H | 5.92150 | 5.08881 | 0.94407 | H | 0.09533 | 2.52721 | 3.63581 |
| C | 9.86974 | 9.18704 | 2.93638 | H | 1.21602 | 2.54388 | 4.99749 |
| H | 10.20967 | 10.03899 | 2.35797 | C | 5.64927 | 2.13427 | 10.48239 |
| C | 5.10965 | 5.82713 | 10.21327 | H | 5.49886 | 1.06338 | 10.64475 |
| H | 4.99584 | 5.65929 | 11.27637 | H | 4.69538 | 2.63194 | 10.66461 |
| C | 1.70983 | 3.92585 | 3.41596 | H | 6.37037 | 2.47308 | 11.22938 |
| C | 6.12929 | 9.35377 | 6.82369 | C | 3.71598 | 10.08517 | 6.75468 |
| H | 6.59696 | 10.29220 | 6.50903 | H | 3.81940 | 10.28560 | 5.69380 |
| H | 6.80408 | 8.86062 | 7.52625 | C | 3.31388 | 9.40943 | 10.99314 |
| C | 3.99475 | 6.11702 | 9.43187 | H | 4.09461 | 8.74816 | 11.37325 |
| H | 3.00823 | 6.19109 | 9.87044 | H | 2.33965 | 8.99406 | 11.25849 |
| C | 9.64421 | 9.32891 | 4.30128 | H | 3.40979 | 10.36399 | 11.51824 |

| | | | |
|---|---|---|---|
| C | 2.49678 | 10.30383 | 7.38366 |
| H | 1.65345 | 10.67785 | 6.81532 |

$[Fe(\mathbf{L})_2]^{2+}$ (S=2)

99

Energy=-3373.614568937

| | | | |
|---|---|---|---|
| Fe | 5.52387 | 6.44859 | 5.62784 |
| N | 7.45742 | 5.72853 | 6.41273 |
| N | 5.80588 | 6.65926 | 3.57083 |
| N | 5.10631 | 4.44267 | 4.75151 |
| N | 5.25360 | 6.22461 | 7.68062 |
| N | 3.42730 | 7.02799 | 6.02454 |
| N | 6.09645 | 8.57682 | 5.31316 |
| C | 6.13003 | 7.85611 | 3.06895 |
| C | 6.26842 | 5.79230 | 8.43907 |
| C | 5.78354 | 2.78800 | 6.41185 |
| C | 4.68881 | 3.24218 | 5.47686 |
| H | 4.41648 | 2.45160 | 4.77013 |
| H | 3.79907 | 3.50496 | 6.05099 |
| C | 5.64786 | 5.60049 | 2.77055 |
| C | 9.22291 | 7.00724 | 3.64221 |
| H | 9.04036 | 6.14794 | 3.00346 |
| C | 8.67541 | 5.54970 | 5.62405 |
| H | 8.45153 | 4.83601 | 4.82980 |
| H | 9.47160 | 5.12827 | 6.24665 |
| C | 4.06658 | 6.51344 | 8.22844 |
| C | 9.08836 | 6.87246 | 5.02155 |
| C | 5.54480 | 2.69703 | 7.78017 |
| H | 4.56047 | 2.94607 | 8.16579 |
| C | 7.48725 | 5.52615 | 7.67565 |
| H | 8.38014 | 5.17262 | 8.18943 |
| C | 5.24088 | 4.38558 | 3.48150 |
| H | 5.04115 | 3.47721 | 2.91382 |
| C | 1.78523 | 4.99680 | 4.56021 |
| H | 1.56807 | 4.89593 | 5.61976 |
| C | 9.34490 | 7.96847 | 5.84526 |
| H | 9.26514 | 7.87059 | 6.92247 |
| C | 2.23648 | 6.22219 | 4.06538 |
| C | 3.07291 | 6.96077 | 7.25173 |
| H | 2.06722 | 7.21543 | 7.58332 |
| C | 6.12891 | 5.63988 | 9.81624 |
| H | 6.96028 | 5.29080 | 10.41479 |
| C | 9.60384 | 8.21888 | 3.06205 |
| C | 6.30153 | 8.89185 | 4.09128 |
| H | 6.61328 | 9.89170 | 3.79098 |
| C | 6.14832 | 6.94575 | 0.85676 |
| H | 6.28105 | 7.05934 | -0.21179 |
| C | 6.53849 | 2.27643 | 8.66723 |
| C | 7.04022 | 2.44895 | 5.91149 |
| H | 7.23275 | 2.49215 | 4.84484 |
| C | 5.83022 | 5.70166 | 1.39330 |
| H | 5.70681 | 4.83332 | 0.75901 |
| C | 9.82850 | 9.31228 | 3.90496 |
| H | 10.12638 | 10.26324 | 3.47692 |
| C | 4.89728 | 5.93034 | 10.39548 |
| H | 4.75722 | 5.81491 | 11.46284 |
| C | 1.59449 | 3.89731 | 3.72652 |
| C | 6.25711 | 9.59761 | 6.35003 |
| H | 6.68070 | 10.50994 | 5.91747 |
| H | 6.96632 | 9.20822 | 7.08184 |
| C | 3.84576 | 6.36913 | 9.59526 |
| H | 2.87930 | 6.60550 | 10.02128 |
| C | 9.71088 | 9.18573 | 5.28519 |
| H | 9.91787 | 10.03616 | 5.92373 |
| C | 2.43978 | 7.38691 | 5.00652 |
| H | 2.83151 | 8.24295 | 4.45500 |
| H | 1.50001 | 7.68756 | 5.48066 |
| C | 6.29387 | 8.04470 | 1.69957 |
| H | 6.54361 | 9.02158 | 1.30635 |
| C | 7.80047 | 1.97277 | 8.14798 |
| H | 8.58814 | 1.64551 | 8.81769 |
| C | 8.04712 | 2.04917 | 6.78063 |
| H | 9.02297 | 1.78099 | 6.39368 |
| C | 2.49075 | 6.35742 | 2.70495 |
| H | 2.82216 | 7.31048 | 2.30718 |
| C | 9.81391 | 8.33369 | 1.57762 |
| H | 9.31164 | 7.52842 | 1.03942 |
| H | 10.87963 | 8.27137 | 1.33992 |
| H | 9.45710 | 9.29203 | 1.19453 |
| C | 1.87497 | 4.04977 | 2.36327 |

| | | | |
|---|---|---|---|
| H | 1.72721 | 3.21097 | 1.69187 |
| C | 4.78248 | 9.67336 | 8.38966 |
| H | 5.63340 | 9.33535 | 8.97417 |
| C | 4.93139 | 9.87055 | 7.01979 |
| C | 2.30738 | 5.26914 | 1.85608 |
| H | 2.48961 | 5.37620 | 0.79310 |
| C | 3.56712 | 9.91702 | 9.03352 |
| C | 2.48398 | 10.34249 | 8.25885 |
| H | 1.52997 | 10.53692 | 8.73660 |
| C | 1.07144 | 2.59360 | 4.26461 |
| H | 1.62676 | 1.74372 | 3.86163 |
| H | 0.02433 | 2.45532 | 3.98168 |
| H | 1.12645 | 2.55986 | 5.35384 |
| C | 6.24531 | 2.10981 | 10.13271 |
| H | 6.02308 | 1.06279 | 10.35821 |
| H | 5.37836 | 2.69913 | 10.43681 |
| H | 7.10076 | 2.39444 | 10.74904 |
| C | 3.84665 | 10.32685 | 6.27194 |
| H | 3.95523 | 10.50836 | 5.20781 |
| C | 3.44063 | 9.77243 | 10.52494 |
| H | 4.21360 | 9.11712 | 10.93048 |
| H | 2.46067 | 9.38403 | 10.80999 |
| H | 3.55172 | 10.74618 | 11.01073 |
| C | 2.62489 | 10.55574 | 6.89121 |
| H | 1.78232 | 10.91506 | 6.31245 |

$[Zn(\mathbf{L})_2]^{2+}$ (S=0)

99

Energy=-3889.235051972

| | | | |
|---|---|---|---|
| Zn | 5.52526 | 6.44601 | 5.63074 |
| N | 7.51398 | 5.78773 | 6.42161 |
| N | 5.79729 | 6.66298 | 3.57673 |
| N | 5.03500 | 4.44499 | 4.75048 |
| N | 5.25837 | 6.22951 | 7.68486 |
| N | 3.37925 | 6.97295 | 6.01156 |
| N | 6.15917 | 8.57121 | 5.33849 |
| C | 6.17110 | 7.84625 | 3.09209 |
| C | 6.28817 | 5.84724 | 8.43791 |
| C | 5.75043 | 2.82254 | 6.41631 |
| C | 4.64170 | 3.24244 | 5.48047 |
| H | 4.38584 | 2.43909 | 4.78198 |
| H | 3.74816 | 3.48963 | 6.05603 |
| C | 5.58332 | 5.62021 | 2.77740 |
| C | 9.27771 | 7.01966 | 3.64190 |
| H | 9.08124 | 6.15224 | 3.01831 |
| C | 8.74023 | 5.59670 | 5.65091 |
| H | 8.52374 | 4.86750 | 4.86886 |
| H | 9.53206 | 5.18879 | 6.28828 |
| C | 4.06142 | 6.47289 | 8.21582 |
| C | 9.15858 | 6.90658 | 5.02451 |
| C | 5.51977 | 2.73752 | 7.78652 |
| H | 4.53129 | 2.96588 | 8.17450 |
| C | 7.52734 | 5.60452 | 7.68184 |
| H | 8.41534 | 5.27193 | 8.21921 |
| C | 5.15304 | 4.40187 | 3.48317 |
| H | 4.94079 | 3.50446 | 2.90208 |
| C | 1.71241 | 4.95687 | 4.54324 |
| H | 1.49692 | 4.84595 | 5.60213 |
| C | 9.43282 | 8.01275 | 5.82830 |
| H | 9.36567 | 7.93185 | 6.90782 |
| C | 2.16432 | 6.18624 | 4.05969 |
| C | 3.04531 | 6.89509 | 7.23815 |
| H | 2.04143 | 7.13067 | 7.59109 |
| C | 6.15437 | 5.70188 | 9.81659 |
| H | 6.99840 | 5.39661 | 10.42135 |
| C | 9.66214 | 8.21937 | 3.03890 |
| C | 6.37187 | 8.87928 | 4.12097 |
| H | 6.69779 | 9.87266 | 3.81315 |
| C | 6.13163 | 6.95732 | 0.87281 |
| H | 6.26197 | 7.07436 | -0.19584 |
| C | 6.52629 | 2.34645 | 8.67232 |
| C | 7.01263 | 2.50817 | 5.91337 |
| H | 7.19922 | 2.54774 | 4.84556 |
| C | 5.75451 | 5.72506 | 1.39878 |
| H | 5.58156 | 4.87063 | 0.75724 |
| C | 9.90373 | 9.32365 | 3.86219 |
| H | 10.20398 | 10.26576 | 3.41661 |
| C | 4.90744 | 5.93945 | 10.38751 |
| H | 4.76881 | 5.82481 | 11.45539 |
| C | 1.52046 | 3.86515 | 3.69966 |

| | | | | | | | |
|---|---|---|---|---|---|---|---|
| C | 6.30399 | 9.58865 | 6.37720 | C | 3.88027 | 10.27161 | 6.28603 |
| H | 6.71490 | 10.51083 | 5.95316 | H | 3.99196 | 10.45332 | 5.22234 |
| H | 7.01456 | 9.20664 | 7.11195 | C | 3.45885 | 9.71239 | 10.53670 |
| C | 3.83899 | 6.32413 | 9.58271 | H | 4.24591 | 9.07849 | 10.94892 |
| H | 2.86134 | 6.51840 | 10.00456 | H | 2.48752 | 9.29847 | 10.81573 |
| C | 9.79991 | 9.21896 | 5.24557 | H | 3.54027 | 10.68946 | 11.02158 |
| H | 10.01958 | 10.07760 | 5.86870 | C | 2.65144 | 10.48101 | 6.89838 |
| C | 2.37687 | 7.33955 | 5.01286 | H | 1.80637 | 10.82603 | 6.31457 |
| H | 2.76065 | 8.20234 | 4.46623 | | | | |
| H | 1.44156 | 7.63258 | 5.50093 | | | | |
| C | 6.33945 | 8.03990 | 1.72324 | | | | |
| H | 6.63602 | 9.00637 | 1.33716 | | | | |
| C | 7.79253 | 2.06561 | 8.14979 | | | | |
| H | 8.58955 | 1.75964 | 8.81855 | | | | |
| C | 8.03146 | 2.13625 | 6.78101 | | | | |
| H | 9.01110 | 1.88579 | 6.39172 | | | | |
| C | 2.41637 | 6.33424 | 2.70025 | | | | |
| H | 2.74884 | 7.29054 | 2.31117 | | | | |
| C | 9.85910 | 8.30827 | 1.55080 | | | | |
| H | 9.33062 | 7.50887 | 1.02887 | | | | |
| H | 10.92020 | 8.21401 | 1.30296 | | | | |
| H | 9.52381 | 9.27033 | 1.15780 | | | | |
| C | 1.79725 | 4.03059 | 2.33715 | | | | |
| H | 1.64720 | 3.19843 | 1.65803 | | | | |
| C | 4.81515 | 9.63582 | 8.40946 | | | | |
| H | 5.66867 | 9.31420 | 8.99951 | | | | |
| C | 4.96891 | 9.83561 | 7.04041 | | | | |
| C | 2.22919 | 5.25448 | 1.84091 | | | | |
| H | 2.40812 | 5.37202 | 0.77842 | | | | |
| C | 3.59194 | 9.85788 | 9.04587 | | | | |
| C | 2.50611 | 10.26557 | 8.26496 | | | | |
| H | 1.54650 | 10.44470 | 8.73747 | | | | |
| C | 1.00088 | 2.55571 | 4.22701 | | | | |
| H | 1.56107 | 1.71104 | 3.81971 | | | | |
| H | -0.04481 | 2.41484 | 3.94013 | | | | |
| H | 1.05323 | 2.51463 | 5.31612 | | | | |
| C | 6.24303 | 2.18279 | 10.14008 | | | | |
| H | 6.05308 | 1.13139 | 10.37445 | | | | |
| H | 5.35991 | 2.74822 | 10.44272 | | | | |
| H | 7.09155 | 2.49763 | 10.75134 | | | | |